THE ASTROPHYSICAL JOURNAL, 497:388–403, 1998 April 10

EVOLUTION AND NUCLEOSYNTHESIS IN LOW-MASS ASYMPTOTIC GIANT BRANCH STARS. II. NEUTRON CAPTURE AND THE *s*-PROCESS

ROBERTO GALLINO,[1] CLAUDIO ARLANDINI,[1,2,6] MAURIZIO BUSSO,[2] MARIA LUGARO,[1] CLAUDIA TRAVAGLIO,[2] OSCAR STRANIERO,[3] ALESSANDRO CHIEFFI,[4] AND MARCO LIMONGI[5]

Received 1997 March 11; accepted 1997 November 17

ABSTRACT

We present a new analysis of neutron capture occurring in low-mass asymptotic giant branch (AGB) stars suffering recurrent thermal pulses. We use dedicated evolutionary models for stars of initial mass in the range 1 to 3 $M_\odot$ and metallicity from solar to half solar. Mass loss is taken into account with the Reimers parameterization. The third dredge-up mechanism is self-consistently found to occur after a limited number of pulses, mixing with the envelope freshly synthesized ^{12}C and *s*-processed material from the He intershell. During thermal pulses, the temperature at the base of the convective region barely reaches $T_8 \sim 3$ (T_8 being the temperature in units of 10^8 K), leading to a marginal activation of the ^{22}Ne(α, n)^{25}Mg neutron source. The alternative and much faster reaction ^{13}C(α, n)^{16}O must then play the major role. However, the ^{13}C abundance left behind by the H shell is far too low to drive the synthesis of the *s*-elements. We assume instead that at any third dredge-up episode, hydrogen downflows from the envelope penetrate into a tiny region placed at the top of the ^{12}C-rich intershell, of the order of a few 10^{-4} $M_\odot$. At H reignition, a ^{13}C-rich (and ^{14}N-rich) zone is formed. Neutrons by the major ^{13}C source are then released in radiative conditions at $T_8 \sim 0.9$ during the interpulse period, giving rise to an efficient *s*-processing that depends on the ^{13}C profile in the pocket. A second small neutron burst from the ^{22}Ne source operates during convective pulses over previously *s*-processed material diluted with fresh Fe seeds and H-burning ashes. The main features of the final *s*-process abundance distribution in the material cumulatively mixed with the envelope through the various third dredge-up episodes are discussed. Contrary to current expectations, the distribution cannot be approximated by a simple exponential law of neutron irradiations. The *s*-process nucleosynthesis mostly occurs inside the ^{13}C pocket; the form of the distribution is built through the interplay of the *s*-processing occurring in the intershell zones and the geometrical overlap of different pulses.

The ^{13}C pocket is of primary origin, resulting from proton captures on newly synthesized ^{12}C. Consequently, the *s*-process nucleosynthesis also depends on Fe seeds, a lower metallicity favoring the production of the heaviest elements. This allows a wide range of *s*-element abundance distributions to be produced in AGB stars of different metallicities, in agreement with spectroscopic evidence and with the Galactic enrichment of the heavy *s*-elements at the time of formation of the solar system. AGB stars of metallicity $Z \simeq \frac{1}{2}\ Z_\odot$ are the best candidates for the buildup of the *main* component, i.e., for the *s*-distribution of the heavy elements from the Sr-Y-Zr peak up to the Pb peak, as deduced by meteoritic and solar spectroscopic analyses. A number of AGB stars may actually show in their envelopes an *s*-process abundance distribution almost identical to that of the main component. Eventually, the astrophysical origin of mainstream circumstellar SiC grains recovered from pristine meteorites, showing a nonsolar *s*-signatures in a number of trace heavy elements, is likely identified in the circumstellar envelopes of AGB stars of about solar metallicity, locally polluting the interstellar medium from which the solar system condensed.

Subject headings: nuclear reactions, nucleosynthesis, abundances — stars: AGB and post-AGB — stars: evolution — stars: low-mass, brown dwarfs

1. INTRODUCTION

Low-mass asymptotic giant branch (AGB) stars suffering recurrent thermal pulses from the He shell show correlated enhancements of newly synthesized ^{12}C and heavy *s*-elements in their photospheres (Smith & Lambert 1990). These stars, whose envelopes are progressively lost through severe stellar winds, are important contributors to the chemical evolution of the Galaxy, accounting in particular for the *main* component in the solar system, i.e., for all *s*-nuclei from Zr to Pb, and for a substantial fraction of Galactic carbon.

Evolutionary models for AGB stars of initial mass in the range of 1 to 3 $M_\odot$ and solar metallicity have been computed with the FRANEC code (Straniero et al. 1997, hereafter Paper I). Further evolutionary models for 1.5 and 2 $M_\odot$ stars with metallicity $Z = 0.01$ have been computed for the present analysis and will be fully described in a subsequent paper of this series.

After a limited number of pulses, for core mass $M_H \geq 0.60$ $M_\odot$, the convective envelope penetrates into the partially

[1] Dipartimento di Fisica Generale, Università di Torino, Torino, Italy.
[2] Osservatorio Astronomico di Torino, Torino, Italy.
[3] Osservatorio Astronomico di Collurania, Teramo, Italy.
[4] Istituto di Astrofisica Spaziale, CNR, Frascati, Italy.
[5] Osservatorio Astronomico di Roma, Roma, Italy.
[6] Present address: Forschungszentrum Karlsruhe, Institut für Kernphysik, D-76021 Karlsruhe, Federal Republic of Germany.

He-burnt zone at the quenching of each instability, mixing freshly synthesized ^{4}He, ^{12}C, and *s*-processed material to the surface. This mechanism, called *third dredge-up*, is reproduced self consistently with the FRANEC code, allowing us to quantitatively determine the nucleosynthesis yields from AGB winds.

In accordance with the findings of previous authors (e.g., Boothroyd & Sackmann 1988a, 1988b; Busso et al. 1988; Blöcker 1995), the maximum temperature at the bottom of the He-burning convective shell barely reaches $T_8 \sim 3$. In such conditions, the large abundance of ^{22}Ne, deriving from the transmutation of almost all CNO nuclei to ^{14}N during H-shell burning, followed by ^{14}N$(\alpha, \gamma)^{18}$F$(\beta^+\nu)^{18}$O$(\alpha, \gamma)^{22}$Ne in the pulse, is only marginally affected by α captures. The limited release of neutrons via the ^{22}Ne$(\alpha, n)^{25}$Mg channel is insufficient to explain the observed *s*-process enhancements in MS, S, and C stars.

The alternative ^{13}C neutron source, which is easily triggered at lower temperatures, must then play the major role. Although the ^{13}C left behind by the operation of the H shell is largely insufficient to account for the observed *s*-enhancements, a large abundance of ^{13}C nuclei might be produced locally in the ^{12}C-rich intershell by proton capture on ^{12}C, if mixing of a small amount of hydrogen from the envelope is allowed. Despite positive tests presented by Iben & Renzini (1982) and Hollowell & Iben (1988) for AGB stars of low metallicity, showing that partial mixing may be induced by the effect of the increased opacity arising from ^{12}C recombination, this mechanism does not work in disk-metallicity stars (Iben 1983). We remind the reader, however, that at the quenching of each instability the H shell remains inactive for a period of one to several thousand years. When the third dredge-up is at work, a sharp H-He discontinuity is left between the bottom of the convective envelope and the top of the intershell region. This discontinuity should likely be smoothed by chemical diffusion or local instabilities (Iben & Renzini 1983; Gallino et al. 1988). A hydrodynamical treatment is required, and this constitutes a major challenge in *s*-process nucleosynthesis studies. This problem is related to an improvement of our knowledge of how to treat turbulent motions and convection, which in stellar evolutionary models are usually approximated by the mixing-length theory. In this respect, it is important to notice that three-dimensional numerical simulations by Nordlund & Stein (1995) showed that in subphotospheric solar conditions, penetration of downflows into the stable subconvective layers are to be expected at a level of several pressure scale heights. Recent parameterized calculations for AGB stars confirm this possibility (Herwig et al. 1997).

At H reignition, the diffused protons are mostly captured by the abundant ^{12}C through the chain ^{12}C$(p, \gamma)^{13}$N$(\beta^+\nu)^{13}$C. The ^{13}C$(p, \gamma)^{14}$N reaction, although faster than the one above, does not compete with ^{13}C production if the number of available protons per ^{12}C nucleus is small. Consequently, a ^{13}C pocket is formed at the top of the intershell region. This consists of a decreasing profile of ^{13}C, accompanied by production of ^{14}N in the uppermost layers, where protons are more abundant. Later on, the advance in mass of the H-burning shell compresses and heats the ^{13}C reservoir. The temperature in the pocket reaches $T_8 \sim 1$ at the start of the next instability. However, as shown by Straniero et al. (1995), at $T_8 \geq 0.9$ (about 8 keV) all ^{13}C nuclides are already being consumed by α capture via the ^{13}C$(\alpha, n)^{16}$O reaction, releasing neutrons in radiative conditions. The large concentration of ^{13}C allows a very efficient *s*-process nucleosynthesis to occur in a tiny radiative zone.

A new, detailed description of the build-up of the *s*-elements in AGB stars is then necessary. Indeed, previous analyses were made under the assumption that neutrons were released in convective conditions, after engulfment of the ^{13}C pocket by the growing thermal instability (Iben & Renzini 1982; Hollowell & Iben 1988, 1989; Gallino et al. 1988; Käppeler et al. 1990).

During recurrent pulses, the highly *s*-enriched pocket is first mixed with material already *s*-processed by previous episodes and then diluted with fresh Fe seeds and H-shell–burning ashes. In the pulse, a second small burst of neutrons is induced by the marginal activation of the ^{22}Ne source, leading to important modifications of *s*-branching dependent nuclei. The efficiency of this second irradiation varies with pulse number, owing to the slight increase of the maximum bottom temperature in the pulse. Consequently, the *s*-nucleosynthesis has to be followed with great care. It is through the interplay of the double neutron pulse mechanism and recurrent thermal instabilities, followed by third dredge-up episodes, that newly synthesized ^{12}C and *s*-processed matter is brought to the envelope and then progressively lost in the interstellar medium by efficient stellar winds, while the central core finds its way toward the white dwarf stage.

The ^{13}C pocket is of *primary* origin, being synthesized directly in the star, starting from hydrogen and freshly made carbon. Consequently, once a ^{13}C profile is chosen, the *s*-process efficiency varies strongly with stellar metallicity. This makes the ^{13}C neutron source in AGB stars a unique tool (Clayton 1988; Gallino et al. 1988; Gallino 1989) for investigating the Galactic enrichment of the heavy *s*-elements.

Because of our present inability to quantitatively estimate the hydrogen downflows in the He intershell, both the extension and the chemical profile of the ^{13}C pocket must be treated as relatively free parameters. A large set of different parameterizations of the ^{13}C pocket have been attempted, and a full discussion will be presented elsewhere. However, as we will discuss in § 2, a number of general constraints exist, including the production ratios of ^{13}C and ^{14}N, which are determined by proton capture rates of ^{12}C and ^{13}C, respectively.

The aim of this paper is to present a detailed analysis of the *s*-process nucleosynthesis occurring in Galactic disk AGB stars, showing that it is indeed possible to constrain the ^{13}C pocket profile to reproduce the main component and to match spectroscopic observations of *s*-enhanced stars, for which a noticeable dispersion in their *s*-element abundance distributions is observed (Smith & Lambert 1990; Busso et al. 1995; Lambert et al. 1995).

In § 2 we discuss the neutron capture network used in the present calculations, following the neutron irradiations released in the various radiative layers of the pocket, which give rise to highly different *s*-process enhancements. In § 3 we consider the new mechanism for producing a composite distribution of neutron exposures in AGB stars through the interplay of recurrent thermal instabilities. In § 4 the effect of light neutron poisons is briefly analyzed. In § 5 the important role played by the second small neutron burst released by the ^{22}Ne source during thermal instabilities is discussed.

In § 6 we investigate the resulting *s*-process enhancements in the He shell material, cumulatively dredged up into the envelope of AGB stars of solar metallicity. In § 7 we point out how the primary ^{13}C neutron source forces the *s*-process efficiency to vary with metallicity. In § 8 the possibility of reproducing the main component in fine detail in single AGB stars is commented upon. In § 9 an astrophysical interpretation of the *strong* component, an idea originally devised by Clayton & Rassbach (1967) on phenomenological grounds, is advanced. Section 10 contains a short description of the astrophysical implications involved in the recent discovery of circumstellar SiC grains recovered from pristine meteorites. Finally, the main conclusions of this paper are summarized in § 11.

2. NEUTRON CAPTURE BY ^{13}C BURNING IN THE INTERPULSE PERIODS

The *s*-process nucleosynthesis has been performed using a postprocess technique that carefully follows the stellar evolutionary structure up to the tip of the AGB. It accounts for the development of the various convective instabilities and radiative interpulse phases, as well as for the recurrent third dredge-up episodes. Charged-particle interactions between light isotopes in the He intershell are coupled with an extended neutron capture network. Knowing the intershell mass mixed with the envelope at any given third dredge-up episode, we can follow the evolution of the *s*-processed material in the mass-losing envelope. The *s*-distributions in the He intershell and in the envelope vary with time. At the photospheric level, we see at any time a complex abundance distribution, derived by integration over all the previous third dredge-up episodes and diluted over the original composition, taking into account the continuous mass loss by stellar winds and the growth of the core mass.

2.1. *Neutron Capture Network*

For the neutron capture network, we use Maxwellian averaged cross sections from Beer, Voss, & Winters (1992a), who included a proper estimate of the temperature dependence. These cross sections have been updated with a large number of experimental measurements and theoretical estimates. For heavy isotopes, these include ^{87}Rb (Jaag & Käppeler 1996a), Sn and Sb isotopes (Käppeler et al. 1993; Wisshak et al. 1996a, 1996b), Te isotopes (Wisshak et al. 1992), $^{134-137}Ba$ (Voss et al. 1994; Voss, Wisshak, & Käppeler 1995; Koehler et al. 1996), ^{138}Ba (Beer, Corvi, & Athanassopulos 1993; Beer, Corvi, & Mutti 1997), Ce and Pr isotopes (Käppeler et al. 1996), Nd and Pm isotopes (Toukan et al. 1995), Sm isotopes (Wisshak et al. 1993), Gd isotopes (Wisshak et al. 1995), ^{155}Eu (Jaag & Käppeler 1995), ^{163}Ho (Jaag & Käppeler 1996b), Ta isotopes (Németh, Käppeler, & Reffo 1992), ^{208}Pb (Corvi et al. 1995, Beer et al. 1997), and ^{209}Bi (Mutti 1997). New measurements are under way, among which are more precise determinations of cross sections of the neutron magic and *s*-only ^{142}Nd, and of its neighbor ^{144}Nd (Wisshak et al. 1997; Guber et al. 1997). Data for cross sections of unstable isotopes not included in Beer et al. (1992a), for which only theoretical estimates are available, are from Holmes et al. (1976).

For all isotopes, stellar factors accounting for the population of ground-level and low-lying excited states at the temperatures involved are derived from Holmes et al. (1976).

The nuclear network extends to all light species below Fe, which act as neutron poisons for the buildup of the *s*-elements. Again, we use cross sections from Beer et al. (1992a), updated for ^{12}C (Ohsaki et al. 1994), ^{14}C (Beer et al. 1992b), ^{15}N (Meissner et al. 1996b), ^{16}O (Igashira et al. 1995), ^{18}O (Meissner et al. 1996a), and ^{22}Ne (Beer et al. 1991). In addition, the 30 keV cross section of ^{28}Si was renormalized to the Bao & Käppeler (1987) estimate of 2.9 mbarn at 30 keV (H. Beer 1993, private communication).

Important (n, p) and (n, α) channels of a number of isotopes are included. For (n, p) channels, we use experimental rates for ^{14}N (Koehler & O'Brien 1989), ^{26}Al (Koehler et al. 1995), ^{35}Cl (Druyts, Wagemans, & Geltenbort 1994), ^{36}Cl (Schatz et al. 1995), and ^{41}Ca (Wagemans et al. 1993). For (n, α) channels, we take experimental rates for ^{17}O (Schatz et al. 1993), ^{26}Al (Skelton, Kavanagh, & Sargood 1987), ^{33}S (Schatz et al. 1995), and ^{41}Ca (Wagemans, Druyts, & Barthélémy 1995). Other theoretical estimates for (n, p) and (n, α) channels, including $^{37, 39}Ar$, ^{40}K, ^{59}Ni, and ^{65}Zn, are from Woosley et al. (1978).

A proper treatment of isomeric states is performed (Ward, Newman, & Clayton 1976; Ward & Fowler 1980; Németh et al. 1992; Klay et al. 1991). This includes ^{26}Al, ^{85}Kr, ^{121}Sn, ^{176}Lu, and ^{179}Hf.

Weak interaction rates for heavy nuclei are taken from Takahashi & Yokoi (1987), who carefully evaluated temperature and electron density effects at astrophysical conditions. More recent β-decay rates of ^{79}Se are from Klay & Käppeler (1988), and those for ^{176}Lu are from Klay et al. (1991). Below iron, weak interaction rates are from Fuller, Fowler, & Newman (1985, extended version available in electronic form), and from Oda et al. (1994).

On the whole, the *s*-process network contains more than 400 isotopes. It is sufficiently extended to take into account all possible branchings that play even a modest role, especially in the higher neutron density conditions established during the small neutron burst released by the $^{22}Ne(\alpha, n)^{25}Mg$ reaction.

2.2. *Choice of the ^{13}C Pocket Profile*

As discussed in § 1, since the first occurrence of the third dredge-up (after nine to eleven pulses, depending on the mass), we have to assume the existence of hydrogen downflows below the formal convective border of the envelope. We start with an H profile as shown in Figure 1, assumed to be characteristic of all the interpulse phases. The ensuing ^{13}C and ^{14}N profiles at H reignition, using Caughlan & Fowler (1988) rates for proton captures on ^{12}C and ^{13}C, are also plotted in Figure 1, where the ^{13}C pocket has been subdivided into three different zones according to the strength of the characteristic neutron irradiation (see below).

The mass of the ^{13}C pocket is $5.0 \times 10^{-4}\ M_\odot$, about 1/20 of the typical mass involved in a thermal pulse. It contains $2.8 \times 10^{-6}\ M_\odot$ of ^{13}C and $9 \times 10^{-8}\ M_\odot$ of ^{14}N. The profile is not very different from the one evaluated by Hollowell & Iben (1988), although we restrict ourselves to hydrogen mass fractions below $X_H \simeq 0.0015$, i.e., to number ratios $N(H)/N(^{12}C) \leq 0.1$. A higher hydrogen abundance would not produce a correspondingly higher abundance of ^{13}C, because of the increasing competition by ^{14}N production. Actually, a large spectrum of ^{13}C profiles is to be

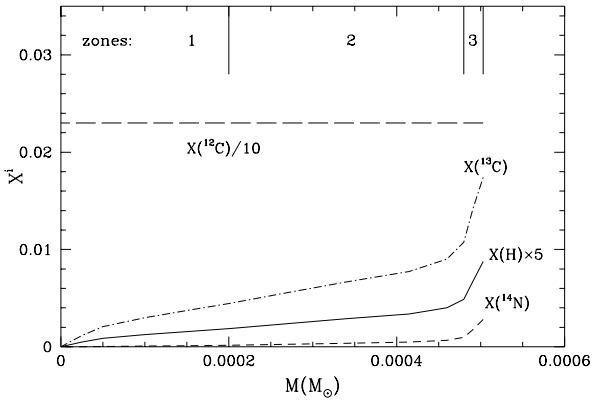

FIG. 1.—The adopted distribution in the mass of hydrogen introduced in the ^{12}C-rich intershell, and of the resulting ^{13}C and ^{14}N profiles at H-shell reignition, as discussed in the text.

expected, as demonstrated by spreads in the *s*-process enhancements of chemically peculiar Population I stars.

2.3. *On Neutron Irradiation in the Radiative* ^{13}C*-burning Layers*

All ^{13}C nuclei available below the H shell are consumed by the ^{13}C(α, n)^{16}O reaction in radiative conditions before the growth of the next instability. Figure 2 (*solid line*) shows the timescale for α capture on ^{13}C versus temperature for a characteristic value of $\rho X_\alpha = 5000$ g cm^{-3}, according to the experimental determination of Denker et al. (1995); in the temperature range of interest, this rate is up to a factor of 2 higher than the previous one (*dashed line*) estimated by Caughlan & Fowler (1988), making the ^{13}C exhaustion occur a bit faster.

The duration of the ^{13}C consumption, including the effect of the delayed neutron recycling by ^{12}C(n, γ)^{13}C(α, n)^{16}O (Travaglio et al. 1996), lasts for about 20,000 yr. This leaves several thousand years before the growth of the next convective instability, which acts to dilute the *s*-processed material over the whole intershell zone.

Figure 3 shows the temporal behavior of the neutron density of three representative layers during ^{13}C consumption. These layers correspond to the middle points of the three zones indicated in Figure 1. The results are given for the 23d interpulse phase (the 15th after the first occurrence of the third dredge-up) of a 3 $M_\odot$ model star of solar composition, mass loss from the Reimers (1975) parameterization with $\eta = 1.15$, as discussed in Paper I. (Note that in Paper I, all η values were mistakenly given at a factor of 2 higher than effectively used.) The neutron density in each layer scales as the ^{13}C local abundance. On the whole, the neutron density is relatively low, reaching $\sim 1 \times 10^7 n$ cm^{-3}. Consequently, only a few branchings along the *s*-path are open. This is illustrated for the same case in Figure 4, where we show the distribution of the $\sigma_i N_i$ products averaged over the ^{13}C pocket as a function of the atomic mass number A. Note the steep decrease in the distribution corresponding to the neutron magic nuclei at $A \sim 90$ ($N = 50$), and at $A \sim 138$ ($N = 82$), as well as the final drop at the double neutron magic ^{208}Pb. A small effect is also apparent at $A \sim 120$, corresponding to the magic charge number $Z = 50$, i.e., to the Sn isotopes.

The neutron exposure achieved in the three characteristic layers discussed above, i.e., the time-integrated neutron flux $\delta\tau^{(i)} = \int N_n v_{\rm th}\, dt$, is 0.13, 0.23, and 0.41 mbarn^{-1}, respectively. The thermal velocity $v_{\rm th}$ is close to 8 keV. The seed material is a combination of fresh Fe seeds, light neutron poisons, and *s*-processed material left in the intershell at the quenching of the previous convective instability. The *s*-process occurring in each layer is highly effective; enhancement factors with respect the initial solar composition for the *s*-only isotopes range from a few thousands up

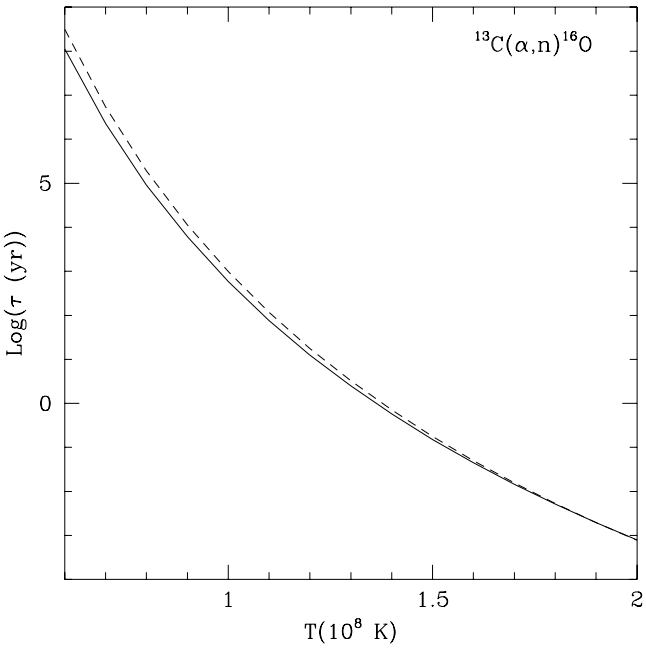

FIG. 2.—Timescale for α captures on ^{13}C for a characteristic value $\rho X_\alpha = 5000$ g cm^{-3}. Solid line shows the experimental rate of Denker et al. (1995); dashed line shows the theoretical evaluation by Caughlan & Fowler (1988).

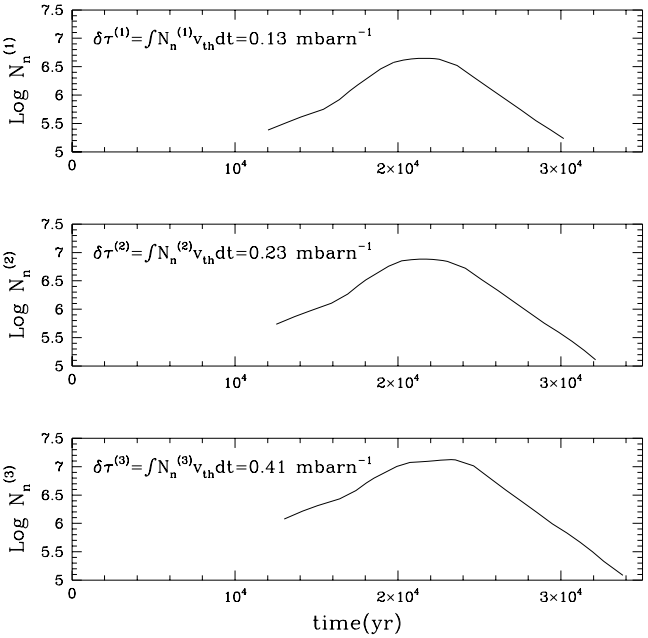

FIG. 3.—Calculated neutron density during ^{13}C consumption in three representative layers of the ^{13}C pocket during the 25th interpulse phase of a 3 $M_\odot$ star of solar metallicity.

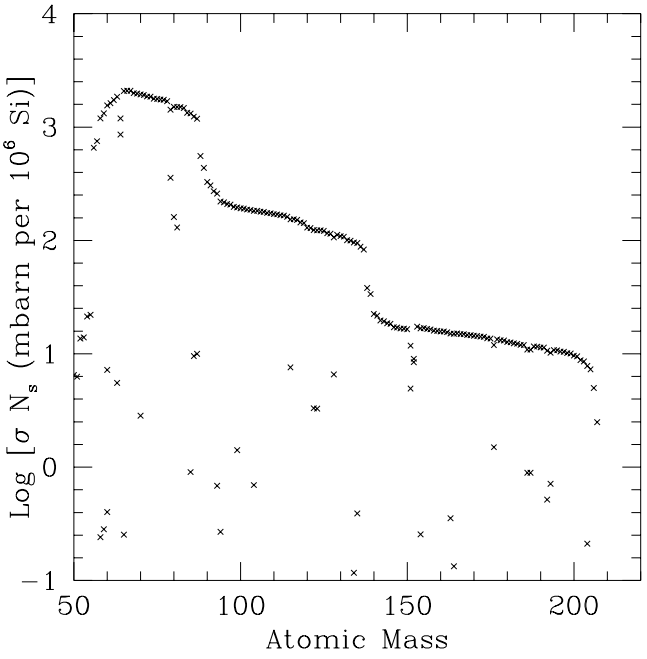

FIG. 4.—Distribution of the $\sigma_i N_i$ products averaged over the ^{13}C pocket as a function of the atomic mass number A. The case is the same as in Fig. 3.

to 50 thousands. As shown in Figure 5, very different enhancement factors are achieved for different values of the local exposure $\delta\tau$ (i.e., in different mass layers), in an extremely nonlinear way.

Actually, the interplay between radiative ^{13}C burning, dilution of the pocket with previous *s*-processed material, mixing with fresh Fe seeds and H burning ashes, and

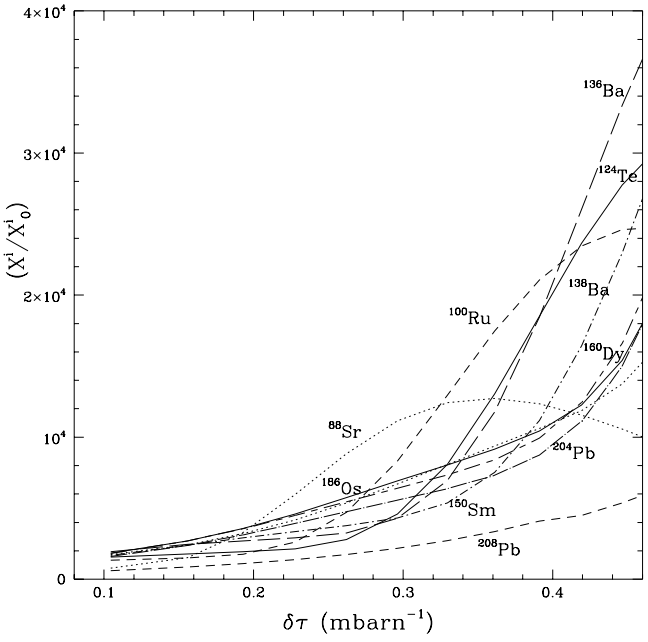

FIG. 5.—Enhancement factors for selected isotopes in different mass layers as a function of the local neutron exposure, for the adopted ^{13}C profile of Fig. 1.

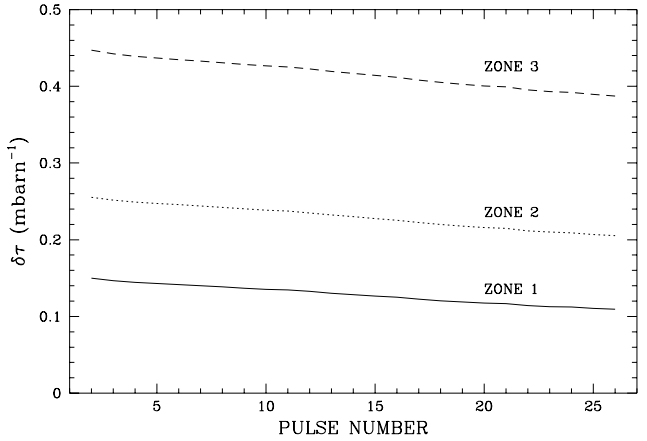

FIG. 6.—Variation of the neutron exposure per interpulse in the three representative layers of Fig. 3.

overlap between successive pulses affects the final abundance distribution. This causes the exposures in each mass zone to change slightly with time, as illustrated in Figure 6, which shows the local neutron exposure in the selected layers of Figure 3 drifting downward with increasing pulse number.

3. THE DISTRIBUTION OF NEUTRON EXPOSURES: A NEW MECHANISM

A key role is played by the recurrent convective instabilities, which dilute the highly *s*-enriched material of the ^{13}C pocket over the whole intershell region. First of all, this allows the next third dredge-up episode to mix ^{12}C-rich and *s*-enriched matter with the envelope. In addition, the neutrons released during each interpulse in the pocket are captured by a mixture of fresh seeds and *s*-processed material from previous cycles.

Figure 7 (*upper panels*) illustrates the development of two subsequent pulses (29th and 30th) for the 3 $M_\odot$ star model discussed so far. The hatched zone represents the region swept by the ^{13}C pocket. The upper solid line (M_{env}) represents the bottom border of the convective envelope, while the line labeled M_H indicates the H/He interface. The lower panel of Figure 7 shows a very schematic representation of the thermal pulse history (see Arlandini et al. [1995] for details). The *s*-processed layers (indicated as a fraction q of the convective pulse) are first diluted over a larger reservoir ($r - q$) containing matter that has suffered previous neutron capture episodes. These are further diluted over the fraction ($1 - r$) with fresh Fe seeds and H-burning ashes. For the sake of simplicity, in this schematic example all geometrical factors are kept constant.

Under the crude assumption that the q layer contains a ^{13}C pocket of uniform composition and undergoes a fixed neutron exposure per interpulse $\Delta\tau$, Figure 8 shows the resulting asymptotic distribution of exposures in the new ^{13}C-burning scenario (*curve 3*). This is to be compared to the Ulrich (1973) mechanism for recurrent overlapping thermal pulses, which give rise to an exponential distribution of neutron exposures (Fig. 8, *curve 1*): $\rho(\tau) \sim (1/\tau_0) \exp^{-\tau/\tau_0}$, the mean neutron exposure τ_0 being $\tau_0 = \Delta\tau/(-\ln r)$, with $\Delta\tau$ being the neutron exposure per pulse and r being the overlap factor between adjacent pulses (both

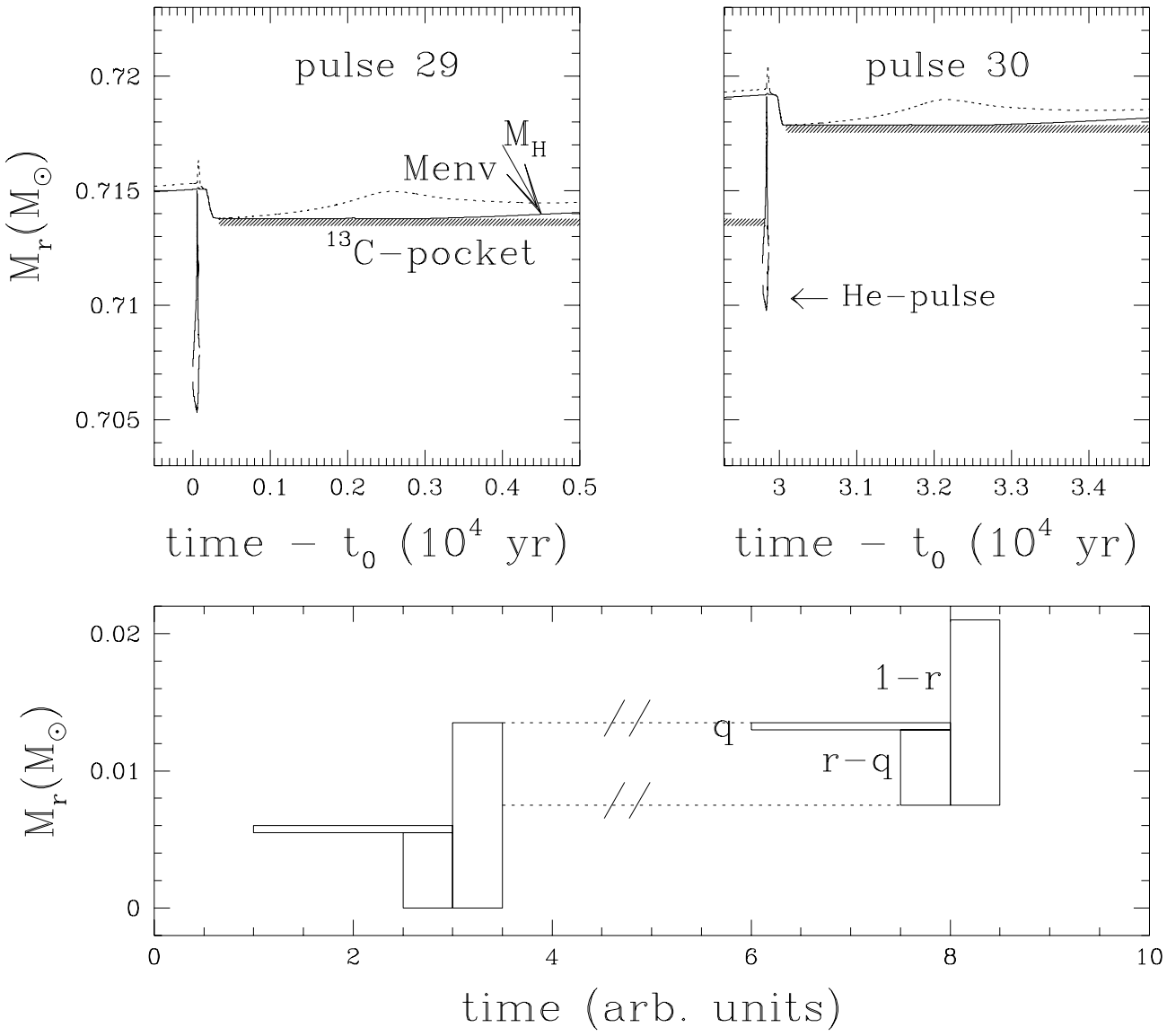

FIG. 7.—*Upper panels*: development of two subsequent pulses (29th and 30th) for the 3 $M_\odot$ star of solar metallicity and Reimers mass-loss parameter $\eta = 1.5$. The hatched zone represents the region swept by the ^{13}C pocket. The upper solid line (M_{env}) represents the bottom border of the convective envelope; the line labeled M_H indicates the H/He interface. *Bottom panel*: schematic representation of the thermal pulse history and *s*-processing in the interpulse periods. The thin *q*-zone indicates the position of the ^{13}C pocket where neutrons are released. The fraction *r* of the mass of the convective He shell contains *s*-processed material from the previous pulses; the fraction $(1 - r)$ contains the H-shell–burning ashes (with fresh Fe seeds) swept by the convective pulse.

assumed to stay constant). Curve 2 represents the distribution of exposures according to the older (now superseded) AGB modeling, in which neutrons were assumed to be released after ingestion of the ^{13}C pocket by the next convective pulse. Again, apart from the scale factor *r*, an exponential distribution of exposures results.

As Figure 8 (*curve 3*) shows, even in the above simplified scenario, the distribution of neutron exposures is much more complex than the usually accepted exponential form, which owed its success to the possibility of obtaining an analytical description, and to the fact that it provided an excellent description of the *s*-abundances, at least with respect to the cross section information available until recently (see Käppeler et al. 1990). Note that, as extensively discussed by Clayton (1968), at a first level of approximation, the abundance distribution of the heavy isotopes ($A \geq 88$) is mainly constrained by the bottleneck effect of neutron magic nuclei at the Sr, Y, Zr peak and the Ba, La, Ce peak, being otherwise controlled by the local criterion $\sigma_i N_i \simeq$ const; it is therefore loosely bound by external conditions. Indeed, Seeger, Fowler, & Clayton (1965) showed that about the same result for the atomic mass range $88 < A < 208$ might be obtained a priori using different distributions of decreasing neutron exposures.

Since then, many improvements have been made. We have high-precision values for a number of critical neutron-capture cross sections, improved solar spectroscopic and CI chondrite abundances (Cameron 1982; Anders & Grevesse 1989; Palme & Beer 1993; Grevesse, Noels, & Sauval 1996), and upgraded evolutionary descriptions of AGB phases. We can then recognize that different distributions of exposures are not really equivalent.

It must be stressed that the example of Figure 8 is an oversimplification of the whole *s*-process history in AGB stars. In the first place, the mass involved in each convective instability decreases with increasing core mass (or pulse

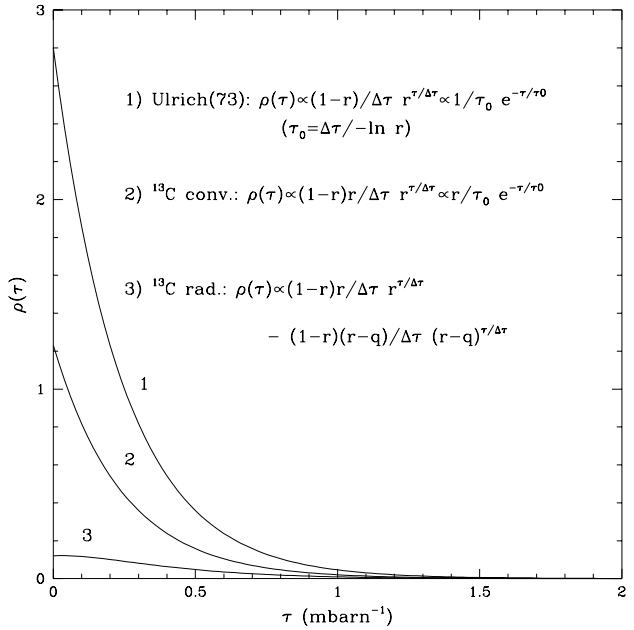

FIG. 8.—*Curve 1*: Asymptotic exponential distribution of neutron exposures $\rho(\tau)$, according to the Ulrich (1973) mechanism of recurrent overlapping thermal pulses. *Curve 2*: Asymptotic exponential distribution of neutron exposures according to the older (now superseded) AGB modeling, with the ^{13}C pocket releasing neutrons after engulfment by the thermal instability. *Curve 3*: Asymptotic distribution of neutron exposures with ^{13}C burning radiatively in the interpulse period according to the simplified scheme of Fig. 7.

number). This is shown in Figure 9*d* for the model star of 3 $M_\odot$. Furthermore, the dilution factor r decreases with pulse number, reaching a constant limit only in the most advanced pulses (Fig. 9*c*). In addition, the small neutron burst driven by the ^{22}Ne source, whose strength varies with pulse number because of variation in the bottom temperature (Fig. 9*b*), makes important modifications to the final *s*-process abundance distribution. Eventually, the *s*-processed material mixed with the envelope and progressively lost by stellar winds shows a different isotopic composition from that left in the He intershell. Indeed, it is the product of the cumulative effect of the various third dredge-up episodes (Fig. 9*a*), each event carrying a different composition of heavy elements.

Another important point not accounted for in Figure 8 is the effect of the neutron captures taking place in the ^{13}C pocket. The ^{13}C radiative burning implies that a composite distribution of exposures is made in the pocket itself, each layer achieving a quite high and different exposure $\delta\tau^{(i)}$. An analytical treatment of this is hardly possible; on the other hand, referring only to an average value of the neutron exposure for each interpulse would yield completely erroneous results. Note that even the usual approximation $\Delta\tau \ll 1$, a necessary condition for obtaining a continuous distribution of exposures (Ulrich 1973), is no longer valid.

Neutrons released by the ^{13}C source under radiative conditions in the interpulse periods of AGB stars make a profound difference to all previous phenomenological mechanisms based on an exponential distribution of exposures. The *s*-process abundance distribution in AGB stars is controlled by the way in which the hydrogen profile penetrates into the ^{12}C-rich intershell. With regard to the effect of the major ^{13}C neutron source, the final abundance distribution is much closer to a superposition of a few single irradiations (Clayton et al. 1961) than to an exponential distribution of exposures.

4. EFFECT OF LIGHT NEUTRON POISONS

The initial composition of the pocket is made up of ^{12}C-rich and, except at its first occurrence, *s*-rich matter from the previous pulse. The isotope ^{14}N, which is commonly considered a strong neutron poison because of its resonant ^{14}N(n, p)^{14}C channel, enters in the radiative ^{13}C burning zone only as a fresh nucleus, synthesized locally together with ^{13}C in the upper layers of the ^{13}C pocket. Indeed, all other ^{14}N nuclei present in the intershell as ashes of HCNO burning in the H shell undergo full conversion to ^{22}Ne in the previous thermal instability. The pocket therefore contains a large abundance of ^{22}Ne, which, however, because of its very low cross section does not appreciably affect neutron captures. Note that the protons released by the above (n, p) channel (and by other minor ones) induce an important delayed neutron recycling through the chain ^{12}C(p, γ)^{13}N($\beta^+\nu$)^{13}C(α, n)^{16}O (Cameron 1955; Jorissen & Arnould 1985, 1989; Gallino 1989). No ^{18}O nuclei, which would efficiently destroy protons through the chain ^{18}O(p, α)^{15}N(p, α)^{12}C, are present in the pocket, since, like ^{14}N, they are destroyed in the previous pulse, in the reaction chain leading to ^{22}Ne production.

Another neutron poison present in great abundance in the ashes of the H-burning shell is ^{26}Al, in its long-lived ground state synthesized by the reaction ^{25}Mg(p, γ)^{26}Al^g (Forestini, Paulus, & Arnould 1991). It has a total (n, p) plus (n, γ) cross section of 164 mbarn at 30 keV. However, in this case a large fraction of ^{26}Al has also undergone substantial depletion by neutron capture in the previous convective pulse.

The above discussion makes it clear that compared to a convective burning scenario, the radiative *s*-process, in which all ^{13}C nuclei are consumed locally and release neutrons without being diluted over the convective pulse, is much less affected by the filtering effect of light neutron poisons.

5. THE DOUBLE NEUTRON PULSE

Figure 9*b* shows the variations from the 9th thermal pulse of the maximum bottom temperature T_{8b} versus core mass for the 3 $M_\odot$ star model of solar metallicity. This illustrates the gradual heating of thermal instabilities up to $T_{8b} \simeq 3.06$ at the end of the AGB phase. Here a second small neutron burst is released by the marginal activation of the ^{22}Ne neutron source. The temporal behaviors of the bottom temperature and density at the maximum growth of selected pulses are illustrated in Figures 10 and 11. These are among the characteristics that have been carefully reproduced in the postprocess code, together with gradients in mass of the temperature and density over the convective instability. The rates of the ^{22}Ne(α, n)^{25}Mg reaction and of the competing channel ^{22}Ne(α, γ)^{26}Mg have recently been revised on experimental grounds. For the (α, n) channel, we use the new rate from Käppeler et al. (1994), after excluding the contribution from an elusive resonance at 633 keV (see also Denker et al. 1995). In the temperature range of interest, these rates are up to a factor of 3 higher than the Caughlan & Fowler (1988) estimates.

The consequences of this second irradiation for the final *s*-process abundance distribution are sensitive, since the *s*-

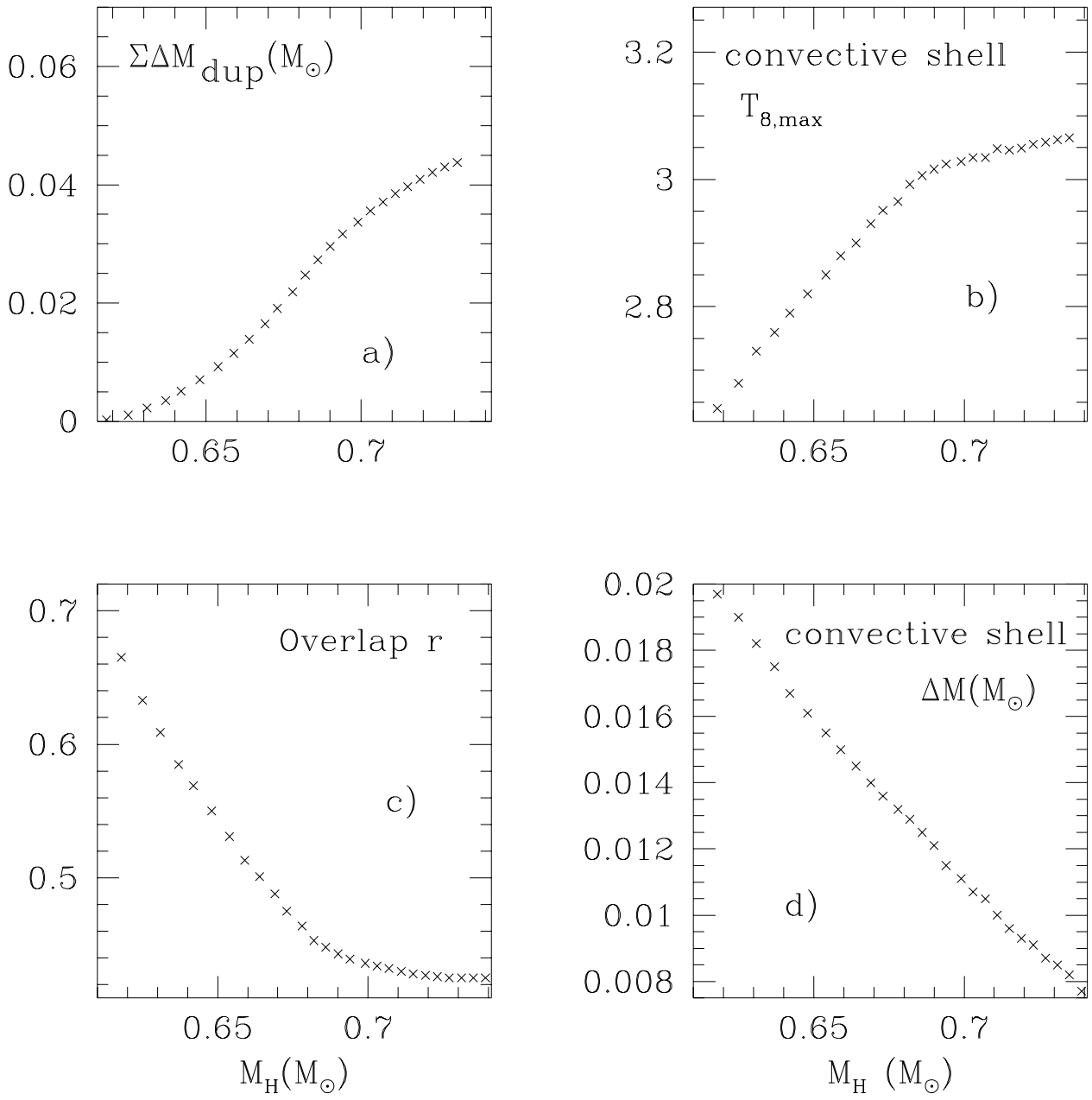

FIG. 9.—Structural and thermodynamical characteristics vs. core mass, M_H (from the 9th thermal pulse on), of the stellar evolutionary model of a 3 $M_\odot$ star of solar composition and Reimers mass-loss parameter $\eta = 1.5$, as discussed in Paper I. (*a*) Cumulative mass dredged up into the envelope. (*b*) Variation of the maximum bottom temperature in the pulses. (*c*) Overlap factor r between subsequent pulses. (*d*) Variation of the convective He shell mass.

processed material present in the *r-q* zone of Figure 8 retains a memory of all previous high-temperature phases.

One important characteristic of the ^{22}Ne source is that the third dredge-up mechanism causes an extra production of primary ^{14}N (and ^{12,13}C) in the H-burning ashes. Indeed, after the occurrence of the third dredge-up, the CNO seeds present in the reactivated H shell are progressively enriched with primary ^{12}C made by partial He burning. Figure 12 shows the variation in the intershell of these three isotopes as a function of the core mass M_H, as obtained from the evolutionary model. For solar metallicity stars, the ^{14}N abundance left behind by the H-burning shell increases by a factor of 2 over the whole AGB phase. Note that these ^{14}N nuclides are fully converted to ^{22}Ne by α capture during each pulse.

Taking this contribution into account and using Maxwellian averaged neutron-capture cross sections and β-decay rates appropriate for these relatively high temperature conditions, Figure 13 shows the resulting average neutron density profile driven by the ^{22}Ne source for selected pulses.

The contribution of the second neutron exposure to the total neutron irradiation is small, ranging from $\delta\tau(20\ \mathrm{keV}) \sim 0.002\ \mathrm{mbarn}^{-1}$ at the 9th pulse to $\delta\tau(23\ \mathrm{keV}) \sim 0.05\ \mathrm{mbarn}^{-1}$ in the latest pulses (where an average effective temperature of $\sim$23 keV is estimated). The neutron exposures from the ^{13}C source are, by comparison, stronger by at least an order of magnitude (as illustrated in Fig. 4), although these are concentrated in tiny radiative layers.

As has already been discussed in Käppeler et al. (1990), the neutron fluences released in the high-temperature phase

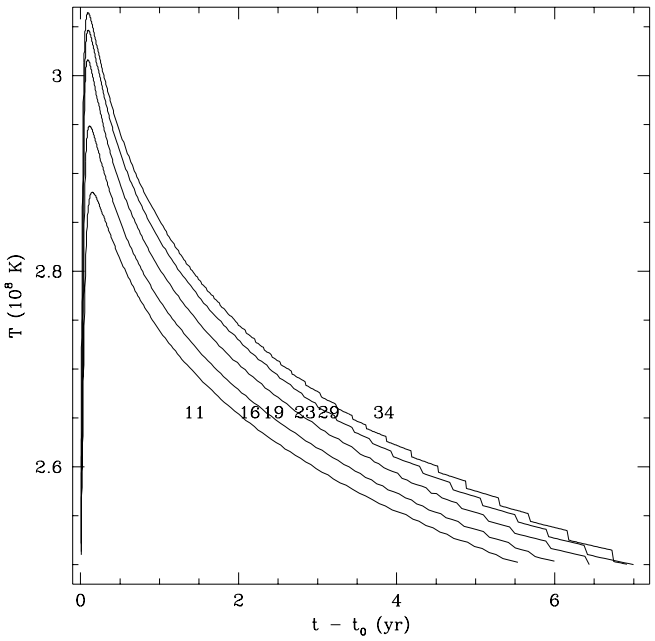

FIG. 10.—Temporal behavior of the bottom temperature in selected convective pulses

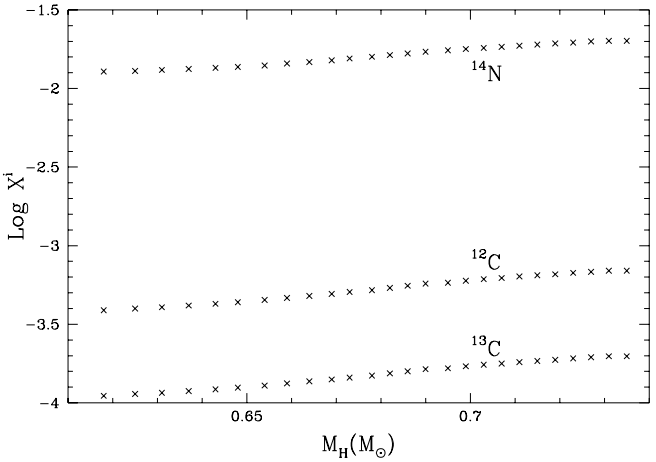

FIG. 12.—Variation of the mass fraction abundances of ^{12,13}C and ^{14}N in the intershell as a function of the core mass M_H.

fix the final abundance of temperature-sensitive branchings, a few of which are only open in this situation. This is the case for the branching at ^{163}Dy (a terrestrially stable isotope), driving the formation of the *s*-only ^{164}Er. The final yields of *s*-only isotopes that depend on branchings along the *s*-path are determined by the freezeout conditions of the neutron fluence (Cosner, Iben, & Truran 1980; Käppeler et al. 1990). This is the case for the pair ^{86,87}Sr and for ^{170}Yb. A new situation arises for magic neutron number nuclides involved in *s*-branchings. These receive a small contribution from the major ^{13}C neutron exposure, but are substantially fed by the ^{22}Ne source, since the neutron density reaches a peak value of up to $\sim 10^{10}$ n cm^{-3}. Characteristic isotopes are ^{87}Rb and ^{96}Zr, and the radiogenic contribution to ^{137}Ba from the decay of ^{137}Cs. The same is true for the neutron-rich and long-lived ^{60}Fe, which has been identified as a live radioactive isotope in pristine solar system material (Shukolyukov & Lugmair 1993). For an account of its possible origin in the winds of a nearby AGB star polluting the placental solar nebula, together with other radioactivities, such as ^{41}Ca and ^{107}Pd, both involved in the *s*-process, we refer to Wasserburg et al. (1994, 1995). An opposite trend is shown by the *s*-branching–dependent ^{134}Ba and ^{152}Gd. These are actually highly overproduced during the major ^{13}C neutron exposure at low neutron density, destroyed during the short ^{22}Ne neutron peak, and eventually restored at branching freezeout conditions, when the neutron density falls below a few $10^8 n$ cm^{-3}. A more detailed description of the double neutron peak effect on *s*-branched isotopes will be discussed elsewhere.

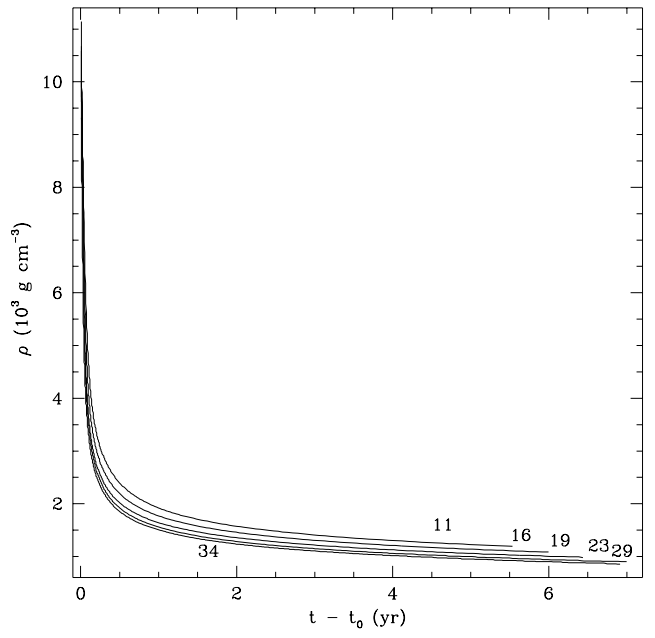

FIG. 11.—Temporal behavior of the bottom density in selected convective pulses

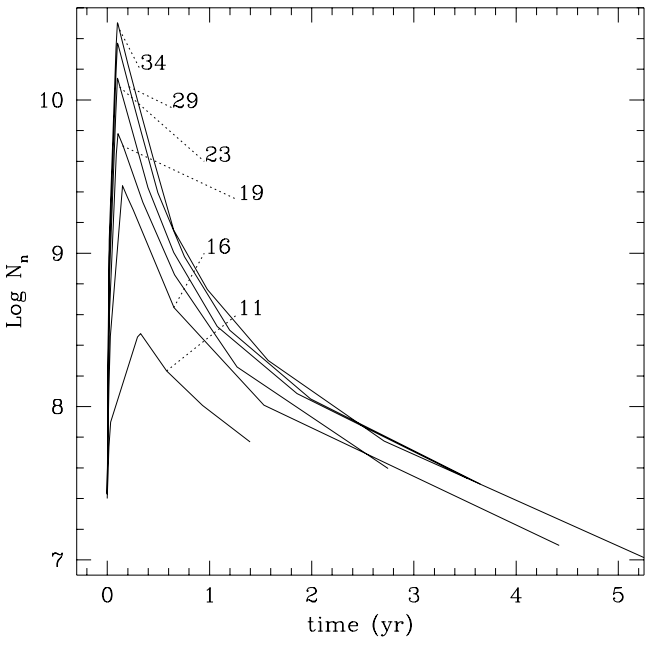

FIG. 13.—Calculated neutron density by the ^{22}Ne source, averaged over the convective zone for different pulses.

6. THE *s*-PROCESS NUCLEOSYNTHESIS IN AGB STARS OF SOLAR METALLICITY

For the 3 $M_\odot$ star of solar metallicity and Reimers mass-loss parameter $\eta = 1.5$, the distribution of the *s*-process abundances in the material carried to the surface, averaged over the mass dredged up by the various mixing episodes, is shown in Figure 14. Filled circles represent *s*-only isotopes; open squares and diamonds indicate isotopes with *s*-contributions higher than 80% and between 60% and 80%, respectively, according to the phenomenological analysis of the main component offered by Käppeler, Beer, & Wisshak (1989). Small crosses are for all other heavy isotopes involved in the *s*-process. Solar abundances used as reference values are from Anders & Grevesse (1989); further updatings marginally affect the solar system abundances of the heavy isotopes. The vertical line marks the limit, in atomic mass number, of the main component. In fact, as first suggested by Clayton & Rassbach (1967) and extensively discussed by Ward & Newman (1978), Walter et al. (1986), and other authors, a quite different distribution of neutron exposures is required in order to reproduce the solar system composition of the *s*-isotopes with $A < 88$, the so-called *weak* component. This is a composite neutron capture process built into massive stars by the ^{22}Ne neutron source partly during core He exhaustion (Lamb et al. 1977; Käppeler et al. 1994) and partly during subsequent convective C- and Ne-shell phases (Raiteri et al. 1993). We shall discuss the strong component later, in § 9.

The resulting abundance distribution shown in Figure 14 is clearly nonsolar. Indeed, in order to reproduce solar abundances, constant enhancement factors for the *s*-only species would be needed, while Figure 14 is characterized by a lower production for heavier nuclei. This was already predictable from the results of Figure 5, in which an important deficiency in the heavy *s*-isotopes beyond the neutron magic number $N = 82$ is evident for any neutron exposure $\delta\tau$. The small exposure from the ^{22}Ne source is incapable of drastically improving the situation. We have then calculated the *s*-process nucleosynthesis for a wider spectrum of single exposures $\delta\tau$. The results are shown in Figure 15. They provide useful guidelines for selecting a ^{13}C profile suitable for reproducing the main component inside a single AGB star. Indeed, there is spectroscopic evidence that *s*-process abundance distributions similar to solar are a common feature of *s*-enhanced stars (Busso et al. 1992, 1995).

Roughly speaking, in order to reproduce the main component one needs a combination of at least two neutron exposures. The first is peaked at around $\delta\tau(8\ \mathrm{keV}) = 0.40\ \mathrm{mbarn}^{-1}$, producing in nearly equal proportions the *s*-only isotopes in the atomic mass region between Zr and Ba. The other exposure, feeding the heavier nuclei, is peaked at around $\delta\tau(8\ \mathrm{keV}) = 0.60\ \mathrm{mbarn}^{-1}$. Both exposures are about a factor of 1.5 times the corresponding exposures reached in zones 2 and 3 of the ^{13}C profile of Figure 1. The match would only be achieved under the condition that the layers suffering the higher exposure were less weighted than those suffering the lower exposure, by about a factor of 10. As a matter of fact, such a different weight is to be expected from a decreasing H profile. The above values of $\delta\tau$ are indicative; their choice is not very critically constrained by the requirement of obtaining a flat distribution of *s*-enhancements. This is so because they are mainly responsible for the build-up of the two major $\sigma_i N_i \sim$ const plateaus along the main component, two regions that are loosely bounded by nuclear constraints, as mentioned in § 3.

Figure 16 shows that an *s*-process abundance distribution nicely reproducing the main component is indeed obtained by simply increasing the previously adopted abundance of ^{13}C by a factor of 2 (with a corresponding modifi-

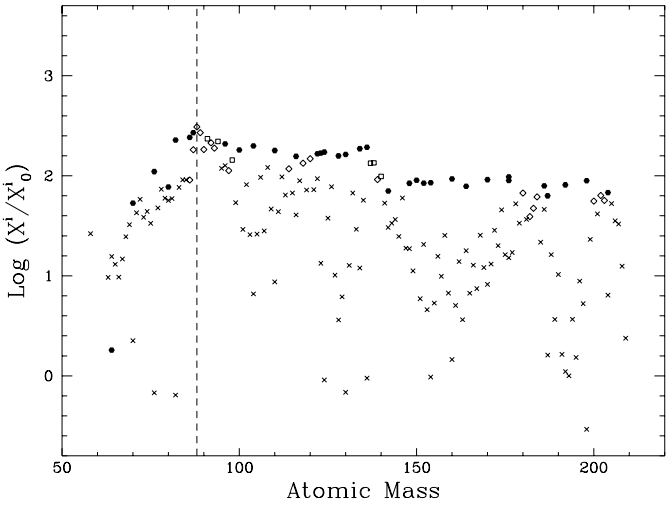

FIG. 14.—Distribution of the *s*-process production factors in the inter-shell matter cumulatively mixed with the envelope by third dredge-up episodes for an AGB star of 3 $M_\odot$, solar metallicity, Reimers mass-loss parameter $\eta = 1.5$, and for the ^{13}C profile of Fig. 1. Solid symbols represent *s*-only isotopes; open squares and diamonds indicate isotopes with *s* contributions higher than 80% and between 60% and 80%, respectively, according to the phenomenological analysis of the main component by Käppeler et al. (1989). Small crosses are for all other heavy isotopes involved in the *s*-process. The vertical line at ^{88}Sr is an eye guide to separate the region of the main *s*-component (the heavier isotopes) from the weak *s*-component. See text for details.

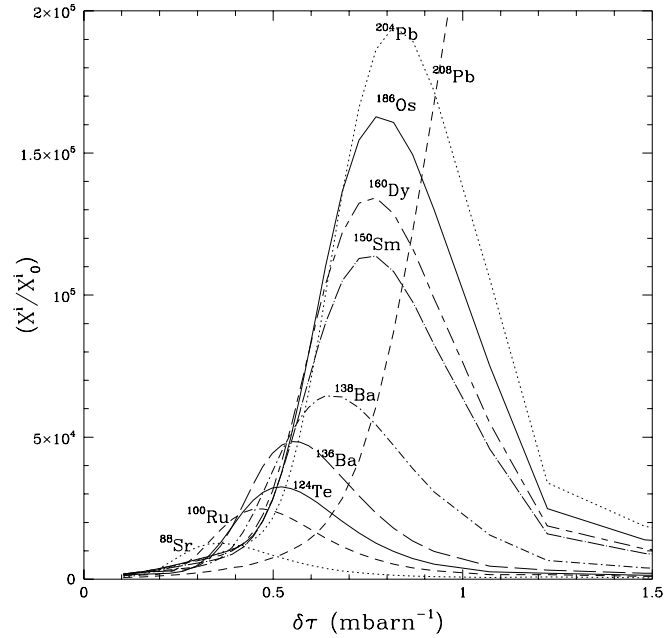

FIG. 15.—Enhancement factors for selected isotopes in different mass layers as a function of the local neutron exposure, for a wider range of single exposures $\delta\tau$ than shown in Fig. 5.

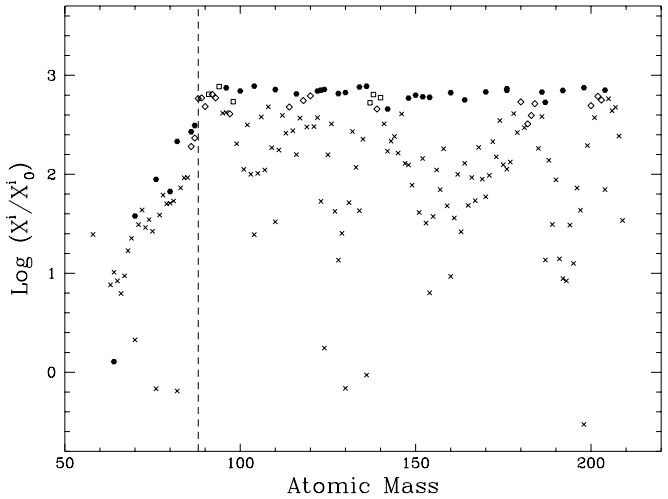

FIG. 16.—Distribution of the *s*-process production factors in the intershell matter cumulatively mixed with the envelope by third dredge-up episodes for the same stellar model of a 3 $M_\odot$ as in Fig. 14, but with a ^{13}C profile increased by a factor of 2, as discussed in the text. The distribution best reproduces the solar main component.

cation of the ^{14}N profile, according to proton capture rates on the C isotopes), without changing the extension in the mass of the pocket. In solar metallicity models, the tail of the ^{13}C profile (zone 1) is of negligible importance for the *s*-process nucleosynthesis.

Up to now, we have investigated the *s*-process nucleosynthesis occurring in a 3 $M_\odot$ star of solar metallicity. For lower masses, we recall that in paper I we did not find the third dredge-up to occur in an AGB star of 1 $M_\odot$, while for the 1.5 $M_\odot$ model with solar metallicity and no mass loss, the third dredge-up was found to occur after the 11th pulse (Fig. 17*a*). Using this stellar model and adopting the same ^{13}C profile as in the 3 $M_\odot$ case discussed before, we obtain about the same final *s*-process abundance distribution, despite the lower integrated dredged-up mass in the envelope. Differences are only seen in a somewhat minor production of the neutron-rich *s*-branched isotopes, such as ^{87}Rb and ^{96}Zr, due to the lower peak neutron density achieved in advanced pulses. Indeed, for lower stellar masses, the slightly lower bottom temperature in the pulse causes the $^{22}Ne(\alpha, n)^{25}Mg$ source to achieve a smaller efficiency. Curiously enough, although the production level of newly synthesized *s* elements in the 1.5 $M_\odot$ AGB star is about a factor of 2 lower than in the 3 $M_\odot$ star, the ^{12}C and *s*-enhacements seen in the envelope in the two cases are almost the same, because the envelope mass and the cumulatively dredged-up mass also change suitably.

Stellar models of 1.5 $M_\odot$ and solar metallicity, computed taking mass loss into account, should in general allow a lower number of third dredge-up episodes.

Note that the higher ^{13}C abundance adopted to reproduce the main component approaches the maximum allowed ^{13}C production from proton capture on ^{12}C, because of the higher production of ^{14}N in zone 3. Consequently, on average, low-mass AGB stars of solar metallicity pollute the interstellar medium with a nonsolar *s*-process abundance distribution, possibly not very different from the one represented in Figure 14.

The results illustrated in Figures 14 and 16 indicate that quite a large spread of *s*-process abundance distributions can be achieved in AGB stars of solar metallicity, including possibly one that reproduces the main component in a single AGB star. This is in agreement with spectroscopic observations. Indeed, AGB stars are known to show different *s*-process abundance distributions; C and S stars with remarkable abundances of elements exist for virtually the same metallicities also observed in MS stars, with relatively small *s*-enrichments. The element distributions also show a rather wide range, from compositions peaked in the Sr-Y-Zr region to more efficient ones rich in Ba, La, Ce, Nd, and Sm (Smith & Lambert 1990; Busso et al. 1992). Other AGB stars, such as the Mira prototype o Cet, show signs of marginal *s*-enrichment only through the presence of Tc.

7. VARIATION OF THE *s*-PROCESS EFFICIENCY VERSUS METALLICITY

We next explore the effect of the initial metallicity on the final *s*-process abundance distribution. We have already mentioned in § 1 that the ^{13}C pocket is of a primary nature, the ^{13}C nuclei being produced directly in the star from proton captures on newly synthesized ^{12}C. Consequently, for a given ^{13}C profile the neutron exposure in disk-metallicity stars scales roughly as the inverse of the metallicity. Complications are introduced in more metal-poor stars by the action of primary-like and secondary-like neutron poisons (Arlandini et al. 1996).

Choosing a metallicity $Z = 0.01$, we ran two evolutionary models, the first for a 1.5 $M_\odot$ star and Reimers mass-loss parameter $\eta = 0.5$, and the second for a $M = 2$ $M_\odot$ star with $\eta = 0.75$. As discussed in Paper I, these choices of the η parameter imply mass-loss rates in the range of those measured for Galactic C stars leaving behind white dwarf remnants, in general accordance with the initial to final mass relation of Weidemann & Koester (1983; see also Weidemann 1987).

The AGB tracks are very similar to those calculated for stars of solar metallicity, as previously found by Boothroyd & Sackmann (1988a, 1988b) and Lattanzio (1986). With the FRANEC code, a limited number of mixing episodes are found for the 1.5 $M_\odot$ star with the adopted mass-loss rate, while the 2 $M_\odot$ star undergoes in all 17 third dredge-up episodes before the envelope mass is sufficiently reduced ($M_{\rm env} \simeq 0.5$ $M_\odot$) to prevent the occurrence of further envelope mixing.

In agreement with the above statements about the primary nature of the ^{13}C source, and adopting the ^{13}C pocket of Figure 1, the *s*-process abundance distribution calculated for the 2 $M_\odot$ star model of $Z = \frac{1}{2}$ $Z_\odot$ shown in Figure 18 is about identical to the one obtained for a solar metallicity AGB star of similar mass after doubling the ^{13}C profile. This result has a rather general application: approximately the same *s*-process abundance distribution results from reducing the metallicity by a given factor with respect to the reference case as is obtained by increasing the ^{13}C in the pocket by the same factor over the reference case (provided that the same profiles of ^{13}C and ^{14}N are adopted). In general, the average *s*-process efficiency will increase toward lower metallicity stars. This expectation is indeed in accordance with spectroscopic observations of Galactic disk CH and Ba stars. Despite the mentioned scatter, these stars, which are on average less metal-rich than the Sun, clearly show higher *s*-process efficiencies than normal MS, S, and C stars, and define an almost linear

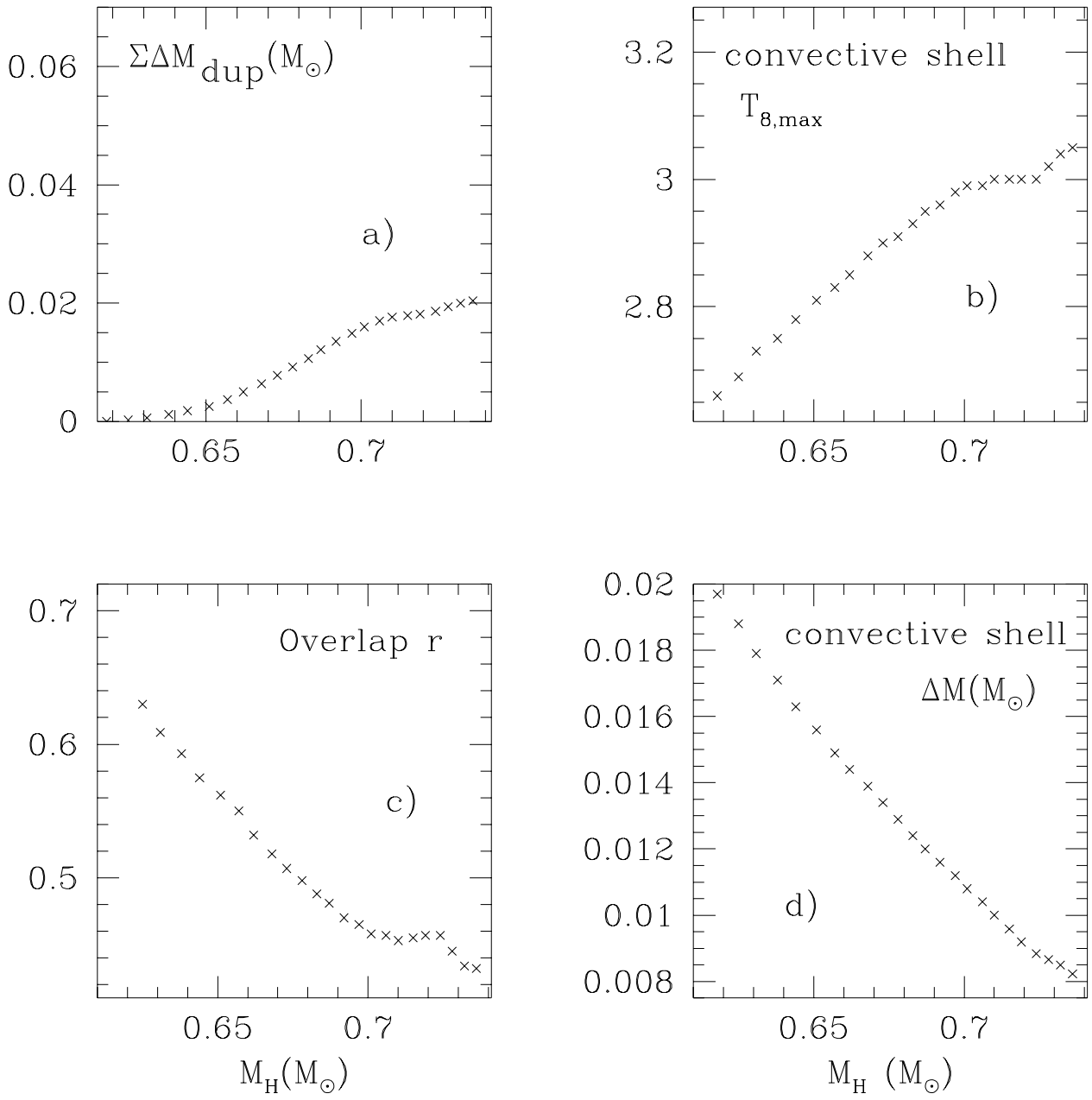

FIG. 17.—Structural and thermodynamical characteristics vs. core mass M_H from the 11th thermal pulse by the stellar evolutionary model of a 1.5 $M_\odot$ star of solar composition and no mass loss, as discussed in Paper I. (*a*) Cumulative dredged-up mass in the envelope. (*b*) Variation of the maximum bottom temperature in the pulses. (*c*) Overlap *r* between subsequent pulses. (*d*) Variation of the mass swept by the convective He shell.

trend of increasing heavy element production with decreasing metallicity (Busso et al. 1996).

Figure 19 shows the *s*-process enhancements in the envelope of the 2 $M_\odot$ AGB model star of metallicity $Z = 0.01$, after cumulative mixing episodes up to the indicated core masses M_H. These correspond to the 5th, 10th, and 17th third dredge-up episodes, respectively. Only pure *s*-isotopes are shown. The distribution is already roughly flat after the first pulses. According to the discussion in § 3, this is a characteristic of ^{13}C burning radiatively in a tiny pocket. The heavier isotopes beyond Ba are synthesized after the first neutron capture episodes in the top layers of the pocket, where the ^{13}C content is higher. Note the progressive decrease of the two branching-dependent isotopes ^{134}Ba and ^{152}Gd with respect to the neighboring ^{136}Ba and ^{154}Gd, respectively.

8. THE MAIN COMPONENT

The result illustrated in Figure 18 constitutes our best fit to the main component. The small spread of the enhancement factors of the heavy *s*-only isotopes is within present uncertainties of solar abundances and neutron capture cross sections. One exception is the neutron magic ^{142}Nd, for which a much lower cross section is needed (see § 10). A small *p* contribution to the unbranched *s*-only isotopes (Howard, Meyer, & Woosley 1991; Prantzos et al. 1990) may account for a slight enhancement in the average mean production factor. It should be stressed that no fitting procedure has been applied; the abundance distribution is obtained in the chosen model star with the assumptions described, and no other constraints or adjustable parameters.

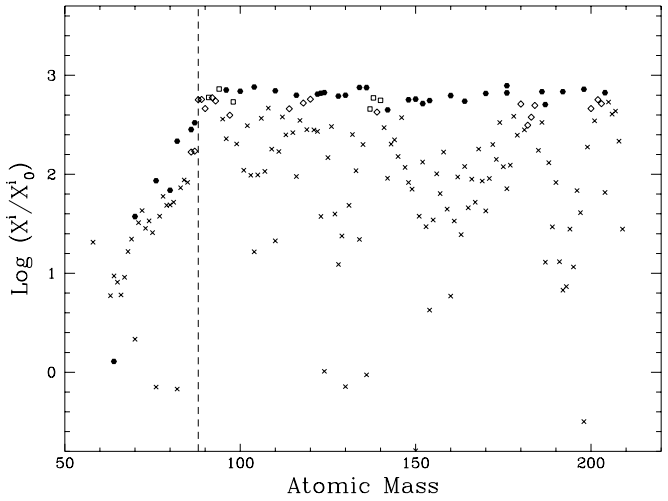

FIG. 18.—Distribution of the *s*-process enhancement factors in the intershell matter cumulatively mixed with the envelope by third dredge-up episodes for a 2 $M_\odot$ star, with metallicity $Z = 0.01$ and $\eta = 0.75$, adopting the ^{13}C pocket profile of Fig. 1. The distribution represents another way to reobtain the main component.

The whole thermal pulse AGB phase lasts for $\sim 2 \times 10^6$ yr. In the stellar photosphere there is a consistent abundance of long-lived isotopes involved in the *s*-path, such as ^{93}Zr and ^{99}Tc (see, e.g., Busso et al. 1992; Lambert et al. 1995). However, in Figure 18 (as well as in Figs. 14 and 16), long-lived isotopes with a half-life lower than 10^7 yr have been allowed to decay to the corresponding stable isobars, to show that the ^{93}Nb and ^{205}Tl solar system abundances have a predominant radiogenic *s*-process contribution.

As discussed in Straniero et al. (1995), the radiatively burning ^{13}C pocket implies that the neutron-rich isotopes ^{86}Kr and ^{87}Rb are substantially underproduced as compared to the *s*-only isotopes, whereas an overproduction was encountered in the previous models based on convective ^{13}C burning (because of the higher neutron density in the pulse; see Käppeler et al. 1990). A lower *s*-production of ^{96}Zr, which depends on the branching at ^{95}Zr in a similar way, is also predicted. The corresponding low Rb/Sr ratio and the Zr isotopic mix predicted by the present models in the envelope are in agreement with recent spectroscopic observations of red giants (Lambert et al. 1995). Furthermore, there is no need to change the solar Sn abundance (by 15%; Wisshak et al. 1996b) or the solar Ba (by 20%; Voss et al. 1994), as is required by phenomenological analysis based on exponential distribution of neutron exposures. Note that a similar discrepancy for Sn is found by Beer et al. (1997), despite the fact that their phenomenological treatment (which assumes a combination of two exponential distributions of exposures) tries to mimic the double neutron pulse scenario, fixing the free "astrophysical parameters" of the two phases (average neutron density, temperature, mean neutron exposure, and overlap factor) to values approaching the conditions in AGB stars that we delineate here. Their suggestion that the problem of Sn can be overcome by assuming a significant *p* contribution for the *s*-only nucleus ^{116}Sn (and for ^{142}Nd) appears unrealistic. The overproduction of ^{134,136}Ba shown in Figure 3 of Straniero et al. (1995) was due to a preliminary analysis of neutron capture taking place in the ^{13}C pocket using a rather rough ^{13}C profile.

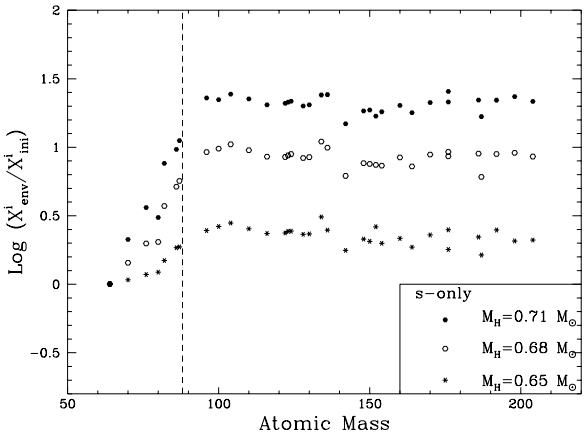

FIG. 19.—Distribution of the *s*-process production factors on the stellar surface after various cumulative third dredge-up episodes up to the indicated core masses M_H. This is obtained for the same ^{13}C pocket profile as in Fig. 3, for a 2 $M_\odot$ model with metallicity $Z = 0.01$ and $\eta = 0.75$.

It must be stressed that in reality, the main component must be interpreted as a suitable mean, performed by Galactic evolution, of different *s*-process nucleosynthesis episodes occurring in disk-metallicity AGB stars. The results shown in Figure 18 represent in this context the case of a star whose *s*-process abundance distribution is closest to that particular average.

The results of § 7 further indicate that the main component derives primarily from stars slightly less metal-rich than the Sun. This expectation is in agreement with spectroscopic observations of Galactic disk C and Ba stars, which on average are less metal-rich than the Sun (Busso et al. 1996).

9. THE STRONG COMPONENT

The trend of the *s*-process versus metallicity in TP-AGB stars, where the neutron exposure increases as the iron content decreases, has an important consequence. Indeed, when the metallicity becomes sufficiently small, the exposures in the pocket become so large that the bulk of nucleosynthesis products shift first past the Zr peak and then past the Ba peak, accumulating at the termination point of the *s*-process, i.e., essentially on ^{208}Pb (and ^{209}Bi). Figure 20 gives the *s*-process abundance distribution calculated with a postprocess code, scaling the metallicity of the previous AGB model star of 2 $M_\odot$ down to [Fe/H] = −1.6, again using the ^{13}C pocket of Figure 1.

Originally, a dedicated *strong* component of the *s*-process was devised (Clayton & Rassbach 1967) for the synthesis of a substantial fraction of Pb not accounted for by the main component, the *r*-process, or radiogenic contributions from transuranic elements (Fowler & Hoyle 1960; Clayton 1964). This strong component now finds a natural interpretation as the low-metallicity equivalent of the same mechanism that in Galactic disk AGB stars is responsible for the main component. This conclusion was anticipated by Gallino et al. (1990a). Note that with updated cross sections, and according to the results illustrated in Figure 18, we predict a contribution of 30% from the main component to solar ^{208}Pb, of 60% to ^{206,207}Pb, and of 100% to the *s*-only ^{204}Pb. Therefore, for ^{208}Pb, whose *r* + radiogenic contribution is estimated to be around 10%, the strong component must account for 60% of the solar abundance.

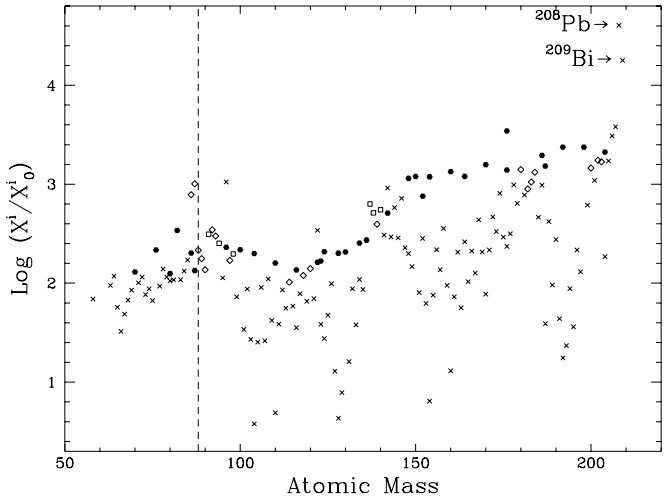

FIG. 20.—Distribution of the *s*-process enhancement factors in the intershell matter cumulatively mixed with the envelope by third dredge-up episodes for a 2 $M_\odot$ star with metallicity scaled to $Z = 0.0005$, adopting the ^{13}C pocket profile of Fig. 1.

Since this huge production of ^{208}Pb at low metallicity occurs as a result of neutron exposures so high that the lighter nuclei (including Ba) are bypassed, we expect the Ba abundance to decrease in very metal poor stars. This is indeed observed in the Galaxy, but the decrease of [Ba/Fe] at very low values of [Fe/H] has so far been interpreted as simply a consequence of the long lifetimes of AGB stars, which implies that at very early times in Galactic history they had not yet started to contribute. We can now recognize that the reason is more complex; indeed, even after the first *s*-process contributions from AGB winds began to appear, they were much more enriched in Pb than in Ba. This also helps to maintain a low Ba abundance in extreme Population II stars if the evolution of the halo was rather long; the consequences of these findings for Galactic chemical evolution require analysis in detail.

10. THE Ne-E(H) ANOMALOUS METEORITIC COMPONENT, CIRCUMSTELLAR SiC GRAINS, AND AGB WINDS

While the envelopes of AGB stars become enriched with newly synthesized ^{12}C and *s* elements from the He intershell by recurrent third dredge-up episodes, reaching C/O > 1 in the more advanced stages, a large circumstellar envelope is formed by efficient stellar winds. Infrared observations clearly show that these envelopes are the site of dust formation. In C-rich environments, the dust feature at 11.2 μm is particularly evident. It is attributed to circumstellar SiC grains that condense at about 1500 K and at C/O $\geq$ 1. A highly anomalous Ne isotopic composition must exist in circumstellar envelopes surrounding C stars. Indeed, the intershell matter brought to the envelope by third dredge-up episodes is highly enriched in ^{22}Ne, deriving from the transmutation of CNO nuclei, first to ^{14}N during H-shell burning, then to ^{22}Ne by α captures in the pulse. This includes the primary ^{14}N abundance resulting from the newly synthesized ^{12}C mixed into the envelope by third dredge-up episodes, then converted to ^{14}N by H-shell burning. A further contribution to ^{22}Ne in the pulse derives from α captures on the radioactive ^{14}C produced in the pocket via the ^{14}N(n, p)^{14}C reaction. On the whole, it is easy to estimate that AGB stars are responsible for the synthesis of about half of the Galactic ^{22}Ne.

It has already been stressed (Gallino et al. 1990b; Lewis, Amari, & Anders 1990) that this process is the origin of the meteoritic Ne-E(H) anomalous component (Black & Pepin 1969), actually carried by circumstellar SiC grains trapped in pristine meteorites (for recent reviews, see Anders & Zinner 1993; Ott 1993; Zinner 1997). The associated *s*-process isotope anomalies in a number of trace heavy elements present in the same grains, among which are Kr, Sr, Zr, Xe, Ba, Nd, S, and Dy, undoubtedly point to their origin in the circumstellar envelopes of AGB stars (Gallino, Busso, & Lugaro 1997).

An improved analysis of the *s*-process signature carried by circumstellar SiC grains is now required. Here we want to stress that on average, the *s*-signature (the *G*-component, according to the definition of Lewis, Amari, & Anders 1990) is nonsolar, showing the characteristics of an average neutron exposure slightly lower than that of the main component (Ott & Begemann 1990a, 1990b; Prombo et al. 1993). We have already shown (Gallino, Raiteri, & Busso 1993) that this *s*-signature is probably due to AGB stars of solar metallicity and masses of 1.5–3 $M_\odot$ locally polluting the protosolar nebula with circumstellar SiC grains. Instead, the average *s*-process abundance distribution in the interstellar medium at that time (i.e., the main component) must have originated in previous generations of Galactic disk stars of lower metallicity.

The high precision attained by ion probes in measuring isotopic ratios of circumstellar SiC grains has developed into a new tool for experimentally investigating the nucleosynthesis occurring in AGB stars. These isotopic measurements are so precise that in a few cases reproducing them by theoretical models yielded predictions with substantial variations in the cross sections. This was the case for the neutron-magic ^{138}Ba and for ^{142,144}Nd (Gallino et al. 1993), comparing the predicted isotope ratios in AGB stars with those of circumstellar SiC grains, measured for Ba by Prombo et al. (1993) and for Nd by Richter, Ott, & Begemann (1993). The first prediction was soon fully confirmed by precise cross-sectional measurements (Beer et al. 1993; Beer et al. 1997). It must be stressed that in this case the Maxwellian cross section of ^{138}Ba at 30 keV remained about unchanged from previous estimates, while an increase of about 40% was found at around 10 keV. Since the final abundance of this neutron magic nucleus essentially depends on the major neutron exposure by the ^{13}C source released at 8 keV, this provides one of the best confirmations of the AGB origin of mainstream SiC grains and of the radiative burning of the ^{13}C neutron source. As for ^{142}Nd, the need for a much lower cross section (by as much as 30%) than reported in the compilation of Beer et al. (1992a) is also evident from its underproduction in the main component (Figs. 16 and 18). Preliminary experimental results for ^{142,144}Nd (Wisshak et al. 1997; Guber et al. 1997) nicely confirm these challenging predictions. A full analysis of the impact of the new Nd cross sections is under way.

These facts should make clear the importance of a careful scrutiny of phenomena such as thermal instabilities and the third dredge-up episodes for meteoritic science.

11. CONCLUSIONS

In this paper we have presented the results of *s*-process calculations for stellar models with a mass range of 1.5 to 3

$M_\odot$, computed with the FRANEC evolutionary code. The major ^{13}C neutron source is activated in radiative conditions in the interpulse phase. The neutron irradiation is characterized by a fairly low neutron density ($N_n \leq 1 \times 10^7$ n cm^{-3}). Various cases have been considered, with varying parameters of either the amount of ^{13}C burnt or the metallicity. A good reproduction of the abundance distribution of the heavy s-nuclei in the solar system can be obtained. The particular choice of the amount of ^{13}C and ^{14}N burnt discussed in the text is obtained for AGB stars of about half the solar metallicity. This fact is in general agreement with spectroscopic evidences of Galactic AGB stars. Virtually the same distribution is obtained in different cases, e.g., scaling the metallicity and the amount of ^{13}C by the same factor. There is, however, a limit for AGB stars of solar metallicity, set by proton-capture rates on C isotopes. The models that reproduce the main component must be seen as a simple way to mimic an abundance distribution that is obtained in nature through Galactic chemical evolution, which generates a suitable average of contributions from stars of different ages and masses.

The small neutron exposure provided in advanced pulses by the marginal activation of the ^{22}Ne neutron source has been taken into account and its effect discussed. Here, the neutron density reaches a peak value of $N_n \geq 10^{10} n$ cm^{-3}. This phase, though characterized by a small neutron irradiation, is nevertheless important for various branchings along the s-path. The s-process contribution to heavy nuclei derived by the combined operation of the two neutron sources has been presented. The new s-process is characterized by a complex distribution of neutron exposures, which can no longer be described in the framework of a phenomenological analysis making use of the concept of exponential distributions of exposures.

The primary nature of the ^{13}C pocket implies an s-process efficiency that varies with stellar metallicity, giving rise to different abundance distributions at different epochs in the Galaxy. A spread of neutron exposures for different ^{13}C profiles is expected in AGB stars at any given metallicity. The strong s-component finds a natural interpretation as the outcome of the neutron captures occurring in very metal-poor AGB stars.

The s-process isotopic signatures of a series of trace heavy elements so far detected in circumstellar SiC grains recovered from pristine meteorites are satisfactorily reproduced within a narrow range of neutron exposures. On average, the s-process signature in circumstellar SiC grains is nonsolar, requiring slightly lower neutron exposures than in the case of the main component. This may be accounted for if the local interstellar medium is polluted by dust that is condensed in the circumstellar envelopes of AGB stars of about solar metallicity. The main component itself results from the accumulation in the interstellar medium of contributions from previous generations of AGB stars of lower metallicity.

A wider series of stellar evolutionary calculations with the FRANEC code is under way in order to extend the computations to other masses and metallicities. This will allow us to investigate the s-enhancements in low-metallicity stars, and the debated astrophysical interpretations (Mathews, Bazan, & Cowan 1992; Pagel & Tautvaišienė 1997) of spectroscopic data on s elements in unevolved stars as a function of metallicity (see Gratton & Sneden 1994, and references therein).

We acknowledge Franz Käppeler for fruitful discussions and for his continuous help in updating the neutron capture network. We owe the referee, Brad Meyer, for interesting suggestions.

REFERENCES

Anders, E., & Grevesse, N. 1989, Geochim. Cosmochim. Acta, 53, 197
Anders, E., & Zinner, E. 1993, Meteoritics, 28, 490
Arlandini, C., Gallino, R., & Busso, M. 1996, Mem. Sov. Astron. Italiana, 67, 845
Arlandini, C., Gallino, R., Busso, M., & Straniero, O. 1995, in Proc. 32d Liège Colloq., Stellar Evolution: What Should Be Done, ed. A. Noels, D. Fraipont-Caro, M. Gabriel, N. Grevesse, & P. Demarque (Liège: Univ. de Liège), 447
Bao, Z. Y., & Käppeler, F. 1987, At. Data Nucl. Data Tables, 36, 411
Beer, H., Corvi, F., & Athanassopulos, K. 1993, in Proc. 8th Int. Symp. on Capture Gamma-Ray Spectroscopy, ed. J. Kern (Singapore: World Scientific), 698
Beer, H., Corvi, F., & Mutti, P. 1997, ApJ, 474, 843
Beer, H., Rupp, G., Voss, F., & Käppeler, F. 1991, ApJ, 379, 420
Beer, H., Voss, F., & Winters, R. R. 1992a, ApJS, 80, 403
Beer, H., Wiescher, M., Käppeler, F., Görres, J., & Koehler, P. E. 1992b, ApJ, 387, 258
Black, D. C., & Pepin, R. O. 1969, Earth Planet. Sci. Lett., 6, 395
Blöcker, T. 1995, A&A, 297, 727
Boothroyd, A. I., & Sackmann, I.-J. 1988a, ApJ, 328, 653
———. 1988b, ApJ, 328, 671
Busso, M., Gallino, R., Arlandini, C., & Straniero, O. 1996, Mem. Soc. Astron. Italiana, 67, 789
Busso, M., Gallino, R., Lambert, D. L., Raiteri, C. M., & Smith, V. V. 1992, ApJ, 399, 218
Busso, M., Lambert, D. L., Beglio, L., Gallino, R., Raiteri, C. M., & Smith, V. V. 1995, ApJ, 446, 775
Busso, M., Picchio, G., Gallino, R., & Chieffi, A. 1988, ApJ, 326, 196
Cameron, A. G. W. 1955, ApJ, 121, 144
———. 1982, in Essay in Nuclear Astrophysics, ed. C. A. Barnes, D. D. Clayton, & D. N. Schramm (Cambridge: Cambridge Univ. Press), 23
Caughlan, G. R., & Fowler, W. A. 1988, At. Data Nucl. Data Tab., 40, 283
Clayton, D. D. 1964, ApJ, 139, 637
———. 1968, Principles of Stellar Evolution and Nucleosynthesis (Chicago: Univ. Chicago Press), 568
———. 1988, MNRAS, 234, 1
Clayton, D. D., Fowler, W. A., Hull, T. E., & Zimmerman, B. A. 1961, Ann. Phys., 12, 331
Clayton, D. D., & Rassbach, M. E. 1967, ApJ, 148, 69
Corvi, F., Mutti, P., Athanassopulos, K., & Beer, H. 1995, in Nuclei in the Cosmos III, ed. M. Busso., R. Gallino, & C. M. Raiteri (New York: AIP), 165
Cosner, K., Iben, I., Jr., & Truran, J. W. 1980, ApJ, 238, L91
Denker, A., Drotleff, H. W., Grosse, M., Knee, H., Kunz, R., Mayer, A., Seidel, R., Soiné, M., Whör, G., & Hammer, J. W. 1995, in Nuclei in the Cosmos III, ed. M. Busso., R. Gallino, & C. M. Raiteri (New York: AIP), 255
Druyts, S., Wagemans, C., & Geltenborn, P. 1994, Nucl. Phys. A, 573, 291
Forestini, M., Paulus, G., & Arnould, M. 1991, A&A, 252, 597
Fowler, W. A., & Hoyle, F. 1960, Ann. Phys., 10, 280
Fuller, G. M., Fowler, W. A., & Newman, M. J. 1985, ApJ, 293, 1
Gallino, R. 1989, in IAU Colloq. 106, The Evolution of Peculiar Red Giants, ed. H. L. Johnson & B. Zuckerman (Cambridge: Cambridge Univ. Press), 176
Gallino, R., Busso, M., & Lugaro, M. 1997, in Astrophysical Implications of the Laboratory Study of Presolar Materials, ed. T. Bernatowicz & E. Zinner (New York: AIP), 115
Gallino, R., Busso, M., Picchio, G., & Raiteri, C. M. 1990a, in Chemical and Dynamical Evolution of Galaxies, ed. F. Ferrini, J. Franco, & F. Matteucci (Pisa: ETS), 338
———. 1990b, Nature, 348, 298
Gallino, R., Busso, M., Picchio, G., Raiteri, C. M., & Renzini, A. 1988, ApJ, 334, L45
Gallino, R., Raiteri, C. M., & Busso, M. 1993, ApJ, 410, 400
Gratton, R. G., & Sneden, C. 1994, A&A, 287, 927
Grevesse, N., Noels, A., & Sauval, A. J. 1996, in ASP Conf. Ser. 99, Cosmic Abundances, ed. S. S. Holt & G. Sonneborn (San Francisco: ASP), 117
Guber, K. H., Spencer, R. R., Koehler, P. E., & Winters, R. R. 1997, Phys. Rev. Lett., 78, 2704
Herwig, E., Blöcker, T., Schönberner, D., & El Eid, M. 1997, A&A, 324, 81
Hollowell, D. E., & Iben, I., Jr. 1988, ApJ, 333, L25
———. 1989, ApJ, 340, 966

Holmes, J. A., Woosley, S. E., Fowler, W. A., & Zimmerman, B. A. 1976, At. Data Nucl. Data Tables, 18, 305
Howard, W. M., Meyer, B. S., & Woosley, S. E. 1991, ApJ, 373, L5
Iben, I., Jr. 1983, ARA&A, 21, 271
Iben, I., Jr., & Renzini, A. 1982, ApJ, 263, L23
———. 1983, ARA&A, 21, 271
Igashira, M., Nagai, Y., Masuda, K., Ohsaki, T., & Kitazawa, H. 1995, ApJ, 441, L89
Jaag, S., & Käppeler, F. 1995, Phys. Rev. C, 51, 3465
———. 1996a, Phys. Rev. C, 53, 2474
———. 1996b, ApJ, 464, 874
Jorissen, A., & Arnould, M. 1985, in Nucleosynthesis and its Implications on Nuclear and Particle Physics, ed. J. Audouze & N. Mathieu (Dordrecht: Reidel), 303
———. 1989, A&A, 221, 161
Käppeler, F., Beer, H., & Wisshak, K. 1989, Rep. Prog. Phys., 52, 945
Käppeler, F., Gallino, R., Busso, M., Picchio, G., & Raiteri, C. M. 1990, ApJ, 354, 630
Käppeler, F., Schanz, W., Wisshak, K., & Reffo, G. 1993, ApJ, 410, 370
Käppeler, F., Toukan, K. A., Schumann, M., & Mengoni, A. 1996, Phys. Rev. C, 53, 1397
Käppeler, F., Wiescher, M., Giesen, U., Görres, J., Baraffe, I., El Eid, M., Raiteri, C. M., Busso, M., Gallino, R., Limongi, M., & Chieffi, A. 1994, ApJ, 437, 396
Klay, N., & Käppeler, F. 1988, Phys. Rev. C, 38, 295
Klay, N., Käppeler, F., Beer, H., & Schatz, G. 1991, Phys. Rev. C, 44, 2839
Koehler, P. E., & O'Brien, H. A. 1989, Phys. Rev. C, 39, 1655
Koehler, P. E., et al. 1995, in Proc. 10th Int. Symp. on Capture Gamma-Ray Spectroscopy, ed J. Kern (Singapore: World Scientific), 714
Koehler, P. E., Spencer, R. R., Winters, R. R., Guber, K. H., Harvey, J. A., Hill, N. W., & Smith, M. S. 1996, Phys. Rev. C, 54, 1463
Lamb, S. A., Howard, W. M., Truran, W. A., & Iben, I., Jr. 1977, ApJ, 217, 213
Lambert, D. L., Smith, V. V., Busso, M., Gallino, R., & Straniero, O. 1995, ApJ, 450, 302
Lattanzio, J. C. 1986, ApJ, 311, 708
Lewis, R., Amari, S., & Anders, E. 1990, Nature, 348, 293
Mathews, G. J., Bazan, G., & Cowan, J. J. 1992, ApJ, 391, 719
Meissner, J., Schatz, H., Görres, J., Herndl, H., Wiescher, M., Beer, H., & Käppeler, F. 1996a, Phys. Rev. C, 53, 459
Meissner, J., Schatz, H., Herndl, H., Wiescher, M., Beer, H., & Käppeler, F. 1996b, Phys. Rev. C, 53, 977
Mutti, P. 1997, Ph.D. thesis, Universiteit Gent
Németh, Z., Käppeler, F., & Reffo, G. 1992, ApJ, 392, 277
Nordlund, A., & Stein, R. S. 1995, in Proc. 32d Liège Colloq., Stellar Evolution: What Should Be Done, ed. A. Noels, D. Fraipont-Caro, M. Gabriel, N. Grevesse, & P. Demarque (Liège: Univ. de Liège), 75
Oda, T., Hino, M., Muto, K., Takahara, M., & Sato, K. 1994, At. Data Nucl. Data Tables, 56, 231
Ohsaki, T., Nagai, Y., Igashira, M., Shima, T., Takeda, K., Seino, S., & Irie, T. 1994, ApJ, 422, 912
Ott, U. 1993, Nature, 364, 25
Ott, U., & Begemann, F. 1990a, ApJ, 353, L57
———. 1990b, Lunar Planet. Sci., 21, 920
Pagel, B. E. J., & Tautvaišienė, G. 1997, MNRAS, 288, 108
Palme, H., & Beer, H. 1993, in Astronomy and Astrophysics, Landolt Börnstein NS IV, Vol. 3a (Berlin: Springer), 196
Prantzos, N., Hashimoto, M., Rayet, M., & Arnould, M. 1990, A&A, 238, 455
Prombo, C. A., Podosek, F. A., Amari, S., & Lewis, R. S. 1993, ApJ, 410, 393
Raiteri, C. M., Gallino, R., Busso, M., Neuberger, D., & Käppeler, F. 1993, ApJ, 419, 207
Reimers, D. 1975, in Problems in Stellar Atmospheres and Envelopes, ed. B. Baschek, W. H. Kegel, & G. Traving (Berlin: Springer)
Richter, S., Ott, U., & Begemann, F. 1993, in Nuclei in the Cosmos II, ed. F. Käppeler & K. Wisshak (Philadelphia: Inst. of Physics), 127
Schatz, H., Jaag, S., Linker, G., Steininger, R., Käppeler, F., Koehler, P. E., Graff, S. M., & Wiescher, M. 1995, Phys. Rev. C, 51, 379
Schatz, H., Käppeler, F., Wiescher, M., Koehler, P. E., & Trautvetter, H. P. 1993, ApJ, 413, 750
Shukolyukov, A., & Lugmair, G. W. 1993, Science, 259, 1138
Seeger, P. A., Fowler, W. A., & Clayton, D. D. 1965, ApJS, 11, 121
Skelton, R. T., Kavanagh, R. W., & Sargood, D. G. 1987, Phys. Rev. C, 35, 45
Smith, V. V., & Lambert, D. L. 1990, ApJS, 72, 387
Straniero, O., Chieffi, A., Limongi, M., Busso, M., Gallino, R., & Arlandini, C. 1997, ApJ, 478, 332 (Paper I)
Straniero, O., Gallino, R., Busso, M., Chieffi, A., Raiteri, C. M., Salaris, M., & Limongi, M. 1995, ApJ, 440, L85
Takahashi, K., & Yokoi, K. 1987, At. Data Nucl. Data Tables, 36, 375
Toukan, K. A., Debus, K., Käppeler, F., & Reffo, G. 1995, Phys. Rev. C, 51, 1540
Travaglio, C., Gallino, R., Arlandini, C., & Busso, M. 1996, Mem. Soc. Astron. Italiana, 67, 831
Ulrich, R. K. 1973, in Explosive Nucleosynthesis, ed. D. N. Schramm & D. W. Arnett, (Austin: Texas Univ. Press), 139
Voss, F., Wisshak, K., Guber, K., & Käppeler, F. 1994, Phys. Rev. C, 50, 2582
Voss, F., Wisshak, K., & Käppeler, F. 1995, Phys. Rev. C, 52, 1102
Wagemans, C., Barthélémy, R., Druyts, S., & Van Gils, J. 1993, Proc. 7th Workshop on Nuclear Astrophysics, ed. W. Hillebrandt & E. Müller, MPA/P7 (Garching: Max-Planck-Institut für Astrophysik), 132
Wagemans, C., Druyts, S., & Barthélémy, R. 1995, in Nuclei in the Cosmos III, ed. M. Busso., R. Gallino, & C. M. Raiteri (New York: AIP), 169
Walter, G., Beer, H., Käppeler, F., Reffo, G., & Fabbri, F. 1986, A&A, 167, 186
Ward, R. A., & Fowler, W. A. 1980, ApJ, 238, 266
Ward, R. A., & Newman, M. J. 1978, ApJ, 219, 195
Ward, R. A., Newman, M. J., & Clayton, D. D. 1976, ApJS, 31, 33
Wasserburg, G. J., Busso, M., Gallino, R., & Raiteri, C. M. 1994, ApJ, 424, 412
Wasserburg, G. J., Gallino, R., Busso, M., Goswami, J. N., & Raiteri, C. M. 1995, ApJ, 440, L101
Weidemann, V. 1987, A&A, 121, 77
Weidemann, V., & Koester, D. 1983, A&A, 121, 77
Wisshak, K., Guber, K., Voss, F., Käppeler, F., & Reffo, G. 1993, Phys. Rev. C, 48, 1401
Wisshak, K., Voss, F., & Käppeler, F. 1996a, Phys. Rev. C, 54, 2732
Wisshak, K., Voss, F., Käppeler, F., Guber, K., Kazakov, L., Kornilov, N., Uhl, M., & Reffo, G. 1995, Phys. Rev. C, 52, 2762
Wisshak, K., Voss, F., Käppeler, F., & Kazakov, L. 1997, Nucl. Phys. A, 621, 270c
Wisshak, K., Voss, F., Käppeler, F., & Reffo, G. 1992, Phys. Rev. C, 45, 2470
Wisshak, K., Voss, F., Theis, Ch., Käppeler, F., Guber, K., Kazakov, L., Kornilov, N., & Reffo, G. 1996b, Phys. Rev. C, 54, 1451
Woosley, S. E., Fowler, W. A., Holmes, J. A., & Zimmerman, B. A. 1978, At. Data Nucl. Data Tables, 22, 371
Zinner, E. 1997, in Astrophysical Implications of Presolar Materials, ed. T. Bernatowicz & E. Zinner (New York: AIP), 3